RSC Advances

PAPER

View Article Online
View Journal | View Issue

Cite this: *RSC Adv.*, 2025, **15**, 42867

Fe_2O_3/g-C_3N_4/CdS photocatalysts for complete sunlight-active detoxification of the tetracycline antibiotic and Congo red dye in water

Khemika Wannakan,[ab] Sattra Nonthing,[a] Atchawadee Panchakeaw[a] and Suwat Nanan *[a]

A ternary heterojunction based on Fe_2O_3/g-C_3N_4/CdS was synthesized *via* an ultrasonic technique. The synthesized heterostructure was utilized for complete detoxification of the tetracycline (TC) antibiotic and Congo red (CR) dye in water. The three-component photocatalyst displayed the XRD patterns of Fe_2O_3, CdS, and g-C_3N_4, with band gaps of 2.62 eV, 2.47 eV, and 2.60 eV, respectively. The 0.10 weight% Fe_2O_3/g-C_3N_4/CdS heterostructure (denoted as 0.10Fe_2O_3/g-C_3N_4/CdS) provided the smallest photoluminescence intensity, indicating the slowest recombination speed of electron–hole pairs, compared to all the fabricated catalysts. This agrees perfectly with the greatest photoactivity detected in the 0.10Fe_2O_3/g-C_3N_4/CdS heterostructure. A photocatalytic performance of 84% was observed after 4 h of UV-visible light exposure. In addition, 97% removal of TC under natural sunlight was reported. This is assigned to the lowest carrier recombination rate of the ternary photocatalyst, compared to the bare components and the binary photocatalysts. The photodegradation of the pollutant follows the first-order kinetics. A maximum rate constant of 0.0432 min^{-1} was detected. The ternary heterojunction displayed excellent photocatalytic activity even after five cycles. The trapping test indicated that the photo-created holes played a main role in TC detoxification. This research provides a novel route to generate ternary heterojunctions for complete detoxification of the harmful TC drug and CR dye in natural water.

Received 12th July 2025
Accepted 20th October 2025

DOI: 10.1039/d5ra04984a

rsc.li/rsc-advances

1. Introduction

Recently, the contamination of water with harmful pollutants has caused serious problems worldwide.[1] The improper discharge of organic contaminants into water has considerably contributed to water pollution.[2,3] Congo red (CR) is an anionic dye that is widely utilized in the textile industry. The chemical structure of CR, comprising the part of harmful colorants, could have carcinogenic effects on human health.[4,5] The discharge of high contents of the CR dye, particularly beyond the safe level, can lead to high toxicity, high chromaticity, and difficulty in detoxification.[6,7]

Tetracycline antibiotic, denoted as TC, is widely used for the treatment of bacterial infection. The drug is discharged into natural water after utilization.[8] Across the globe, as the growth of the pharmaceutical industry is quite rapid, the misuse of the drug has enhanced the antibiotic level found in the aqueous phase.[9] This will keep increasing to a level higher than the safe level.[10] After discharge, the non-biodegradable property of the TC drug causes the contamination of natural water with its residual parts.[11] The extensive utilization of antibiotics causes the release of these drugs into the environment, which will finally cause a dreadful effect in animals and humans.[12] In practice, it is very important to use, manage and discharge the antibiotic appropriately. Thus, the complete degradation of TC detected in water is of high concern.[13,14]

Various techniques have been applied for the detoxification of antibiotics.[15–17] Some methods, however, face the main difficulty of converting the harmful drugs from the liquid to solid phase. This will eventually lead to the creation of toxic contaminants.[18,19] It is extensively accepted that the United Nations' Sustainable Development Goals (SDGs) are the main goals to be achieved. Goal number 6 (clean water and sanitation) can specifically be achieved by selecting the optimal method to degrade harmful contaminants including drugs, which are detected in the aqueous phase.[20] Among numerous methods, photocatalysis has received much attention owing to the benefits of applying abundant sunlight for complete removal of pollutants.[21,22] It is well known that TiO_2 is a UV-responsive photocatalyst, showing quite low visible-light photoactivity. In principle, the synthesis of sunlight-active catalyst is a much more promising direction in the field of

[a]*Department of Chemistry, Center of Excellence for Innovation in Chemistry (PERCH-CIC), Faculty of Science, Khon Kaen University, Khon Kaen 40002, Thailand. E-mail: suwatna@kku.ac.th; Fax: +66 43 202373; Tel: +66 43 202222 41, ext. 12370*

[b]*Department of Materials Science and Engineering, School of Molecular Science and Engineering, Vidyasirimedhi Institute of Science and Technology (VISTEC), Rayong, 21210, Thailand*

photocatalysis for environmental remediation.[23,24] Practically, the preparation of sunlight-responsive semiconductors with promising photocatalytic activity is the ideal research direction in terms of the synthesis of new catalysts for environmental photocatalysis.[25,26]

Cadmium sulfide (CdS) displays a visible-light-active property with a band energy of 2.2 eV.[1,2,27] However, the combination of electrons and holes was found to be very fast in the bare CdS photocatalyst.[27,28] Moreover, the photo-corrosion problem obstructs the use of the bare CdS photocatalyst.[28] To solve these problems, the preparation of CdS with excellent photoactivity and low photo-corrosion is the first priority.[29]

Graphitic carbon nitride (g-C_3N_4) has drawn much attention owing to the advantages of great thermal, chemical, and structural stability.[30] In addition, the g-C_3N_4 photocatalyst displayed a proper band structure, after generation by the calcination of organic substances including dicyandiamide, urea, thiourea, thioacetamide and melamine.[12,31] The g-C_3N_4 photocatalyst provides a small band gap of around 2.7 eV (visible light). However, application of the pristine g-C_3N_4 photocatalyst for photocatalysis is limited by its low solar-light photoactivity. This is assigned to the poor electron–hole separation at the interface. To improve the final photocatalytic performance of the catalyst, various techniques were utilized to alter the chemical structure of the bare g-C_3N_4 photocatalyst. Particularly, the focus is on lowering the charge recombination. It is noted that g-C_3N_4 displays negative energy band levels, in comparison to the conventional inorganic semiconductors. This is advantageous for the addition of g-C_3N_4, as an excellent candidate for the fabrication of binary or ternary photocatalysts, in combination with other inorganic semiconductors.[32]

Hematite or ferric(III) oxide (Fe_2O_3) is a photocatalyst that can absorb visible light, with a narrow band gap of around 2.1 eV.[33] Nevertheless, the low band gap of Fe_2O_3 results in the fast combination of electron–hole pairs. This limits the real-scale use or the practical application of Fe_2O_3 for environmental remediation.[34] In principle, the combination of Fe_2O_3 with other photocatalysts to generate the novel heterojunctions would be a promising avenue for the improvement of the resulting photoactivity.[35,36]

Principally, applying CdS, g-C_3N_4, or Fe_2O_3 separately will provide a very low photocatalytic performance in terms of detoxification of the contaminant. To solve this drawback, well-distributed silver/gold metals on the catalyst surface or the formation of new heterostructure photocatalysts can be selected.[37–42] It has been reported that the incorporation of noble metals will finally end up with high cost for catalyst preparation. Interestingly, an alternative method based on the creation of new heterojunctions is an excellent choice to increase the photoactivity of the final semiconductor. To generate novel heterostructure photocatalysts, band alignment and band level are the two main parameters that need to be determined.[40–42] The preparation of binary and ternary photocatalysts containing CdS, g-C_3N_4 or Fe_2O_3 has been reported previously.[43–54]

As shown above, in this work we synthesized a novel solar-light-driven Fe_2O_3/g-C_3N_4/CdS photocatalyst *via* a facile ultrasonic route. The prepared 0.10Fe_2O_3/g-C_3N_4/CdS photocatalyst was used for the detoxification of TC antibiotic and Congo red dye. According to the literature, there are some reports on the creation of Fe_2O_3/CdS/g-C_3N_4 photocatalysts.[35,36] However, the application of the prepared catalyst was only for dye degradation. In this work, we used the ternary 0.10Fe_2O_3/g-C_3N_4/CdS photocatalyst for the removal of the TC antibiotic. The novelty is also concerning the facile synthesis based on an ultrasonication route for the preparation of the ternary heterojunction. The presence of Fe_2O_3, g-C_3N_4 and CdS in the ternary heterostructure was confirmed. The 0.10Fe_2O_3/g-C_3N_4/CdS photocatalyst revealed the astonishing increase in the sunlight-driven photoactivity, compared to the bare components and the binary photocatalysts. The improvement in the photoactivity is assigned to the dramatic decrease in the recombination speed of the carriers after the synthesis of the three-component heterostructure. The 0.10Fe_2O_3/g-C_3N_4/CdS photocatalyst displayed excellent reusability even after five cycles. The present research displays a facile technique to generate ternary catalysts with promising photoactivity for the detoxification of harmful pollutants in the environment using the economical solar energy.

2. Experimental

2.1 Materials

All the chemicals used were of AR grade.

2.2 Preparation of photocatalysts

2.2.1 Preparation of CdS. CdS was prepared by a hydrothermal method. A Cd^{2+} solution was prepared by adding 6.1696 g of $Cd(NO_3)_2$ (Loba Chemie Pvt Ltd, AR grade) into 30 cm^3 of water. Meanwhile, a S^{2-} solution was prepared by adding 1.5026 g of thiourea ($(NH_2)_2CS$, HiMedia, AR grade) into 30 cm^3 of water. After that, the S^{2-} solution was added dropwise into the Cd^{2+} solution. The mixture was stirred for 0.5 h and then transferred into an autoclave which was maintained at 120 °C for 12 h. After cooling, the solid was filtered, washed with water and ethanol, and then finally dried at 60 °C for 6 h.

2.2.2 Preparation of g-C_3N_4. The bare g-C_3N_4 photocatalyst was fabricated *via* the calcination of urea (RCI Labscan, AR grade) in the powder form in a muffle furnace. Around 15 g of urea was added to a covered alumina crucible. It was then placed in a muffle furnace at 580 °C for 2 h, with a heating rate of 5 °C min^{-1}. The yellow powders were collected after cooling.

2.2.3 Preparation of Fe_2O_3. Hematite (Fe_2O_3) was prepared by a hydrothermal method. In a typical procedure, 2.4375 g of $FeCl_2$ salt (Qrec, AR grade) was added into 30 cm^3 of water under stirring for 0.5 h. Separately, a solution of 2 M NaOH was prepared. After that, 30 cm^3 of 2 M NaOH was added to the Fe^{2+} solution. It was stirred for 1 h and then loaded into a 100 cm^3 Teflon-lined autoclave that was maintained at 160 °C for 12 h. The precipitate was collected after cooling. It was washed with water and ethanol and dried at 60 °C for 8 h. The solid sample was calcined at 450 °C for 3 h, at a heating rate of 2 °C min^{-1}.

2.2.4 Preparation of the binary photocatalyst. Typically, to synthesize a g-C_3N_4/CdS photocatalyst, 0.2 g of g-C_3N_4 was dispersed in 20 cm^3 of water, for 60 min in an ultrasonic bath. Separately, ultrasonication of CdS (0.2 g) in 20 cm^3 of water was also performed. The CdS dispersion was then added to the g-C_3N_4 dispersion, and the mixture was further ultrasonicated for 2 h. Afterward, 10 cm^3 of acetone was added to the mixture, followed by continuous stirring for 24 h. The solid product was collected *via* filtration. It was washed with water and ethanol and finally dried at 80 °C overnight. The other two photocatalysts, namely, g-C_3N_4/Fe_2O_3 and CdS/Fe_2O_3 heterojunctions were prepared *via* a similar route.

2.2.5 Preparation of the ternary Fe_2O_3/g-C_3N_4/CdS photocatalyst. The Fe_2O_3/g-C_3N_4/CdS photocatalyst was also prepared *via* an ultrasonic route. In practice, about 0.4 g of the g-C_3N_4/CdS binary catalyst was distributed in 30 cm^3 of water, in an ultrasonic bath for 60 min (dispersion A). Meanwhile, the dispersion B was prepared by ultrasonication of Fe_2O_3 (0.05 g of Fe_2O_3 in water). Afterward, the dispersion B was incorporated into the dispersion A. The mixture was continuously ultrasonicated for 2 h. Subsequently, 20 cm^3 of acetone was added to the mixture. It was further stirred for 24 h. Finally, the product was washed with water and ethanol and dried at 80 °C for 24 h. The sample is called 0.05Fe_2O_3/g-C_3N_4/CdS. The other two samples, namely, 0.10Fe_2O_3/g-C_3N_4/CdS and 0.20Fe_2O_3/g-C_3N_4/CdS were also prepared by the same method using 0.10 g and 0.20 g of Fe_2O_3, respectively.

2.3 Characterization

The characterization of the synthesized catalysts was carried out by various techniques. The details can be found elsewhere.[2,8,11,12] The chemical structure of the sample was investigated by X-ray diffraction (XRD) using a PANalytical Empyrean diffractometer (Cu Kα radiation). The vibrational spectrum was examined using a PerkinElmer FT-IR IFS 66 V/S spectrophotometer. The morphological structure based on the SEM micrograph was recorded using an FEI Helios NanoLab G3 CX instrument. The energy-dispersive X-ray (EDX) method was carried out using a TECNAI G2 20 instrument. The UV-visible spectrum was recorded using a Shimadzu UV-Vis-NIR-3101PC spectrophotometer. The $BaSO_4$ salt was utilized as the reference. Finally, the PL spectrum was recorded using a Shimadzu RF-5301PC fluorometer.[2,8,11,12]

2.4 Photocatalytic degradation of the antibiotic

To remove the TC antibiotic, the degradation experiment was conducted using UV-visible light (an LED lamp, 15 W) and natural solar light. Furthermore, the photolysis test was performed by the irradiation of TC antibiotic without the incorporation of the ternary photocatalyst.[8,11,12] In terms of ordinary photocatalytic study, the catalyst (50 mg) was dispersed in a TC aqueous solution (concentration of 10 ppm and total volume of 200 cm^3). To establish the equilibrium of the adsorption/desorption, the mixture was stirred in the dark for 60 min.[12] After photo-illumination, about 5 cm^3 sample was collected at the specific time. The TC concentration was determined by measuring the absorbance at a maximum wavelength of 358 nm by the UV-vis spectrophotometric method.[8,11,12]

The photocatalytic efficiency toward TC removal was determined as follows:

$$\text{Photocatalytic efficiency (\%)} = (1 - C/C_0) \times 100\% \quad (1)$$

where C_0 and C are the initial TC amount and the TC amount at the time of photo illumination, respectively.

The degradation rate was also examined using the following equations:

$$dC/dt = -k_1 C \quad (2)$$

$$\ln(C_0/C) = k_1 t \quad (3)$$

where k_1 is the first-order rate constant.

The detoxification of TC under natural solar light was also investigated in June 2025. The effect of catalyst amount, TC concentration, and solution pH on the degradation efficiency was fully elucidated.[8,11,12] To investigate the main species, playing a crucial role in TC removal, $K_2Cr_2O_7$, isopropanol, NaN_3, and EDTA-2Na were separately used as a quencher of photogenerated electrons, hydroxyl radicals, singlet oxygen atoms, and holes, respectively. In addition, KI was used as a quencher of holes and surface hydroxyl radicals. Each scavenger was incorporated during the study of TC degradation. The recycle of the sample was investigated for five runs.[12]

3. Results and discussion

3.1 Characterization

The crystal structures of the prepared samples were examined by X-ray diffraction (XRD). As shown in Fig. 1a, the XRD patterns of CdS at $2\theta = 24.94°$, 26.44°, 28.31°, 36.83°, 43.78°, 48.03° and 52.01° were assigned to the reflection from the (100), (002), (101), (102), (110), (103) and (112) planes, respectively. This confirmed the hexagonal phase of CdS (JCPDS No. 10-0454).[1,2,6] The pristine Fe_2O_3 photocatalyst displayed peaks at $2\theta = 24.14°$, 33.28°, 35.64°, 40.99°, 49.53°, 54.19°, 62.62° and 64.21° which corresponded to the reflection from the (012), (104), (110), (113), (024), (116), (214) and (300) planes, respectively, indicating the rhombohedral phase of Fe_2O_3 (see JCPDS No. 33-0664).[12] The pristine g-C_3N_4 showed the peak at 27.81° assigned to the reflection from the (002) plane of g-C_3N_4 (see JCPDS No. 87-1526).[12] The binary g-C_3N_4/CdS photocatalyst mainly displayed the peaks from CdS, while the ternary 0.10Fe_2O_3/g-C_3N_4/CdS photocatalyst showed the peaks which are ascribed to CdS and Fe_2O_3. The XRD peak of g-C_3N_4 seems to be quite low and hard to detect, compared to those of CdS and Fe_2O_3. This may be assigned to the low crystallinity property of g-C_3N_4.[12] The confirmation regarding the successful generation of the 0.10Fe_2O_3/g-C_3N_4/CdS photocatalyst will be presented later in terms of FT-IR spectra and EDX analysis.

The FT-IR spectrum of each sample was recorded using an FT-IR spectrophotometer (Fig. 1b). The CdS catalyst showed bands at 3480 cm^{-1} corresponding to the O–H stretching of the adsorbed water on the catalyst surface. The peak at 626 cm^{-1} confirmed the Cd–S bond.[1,2,6] The additional peak at 1120 cm^{-1}

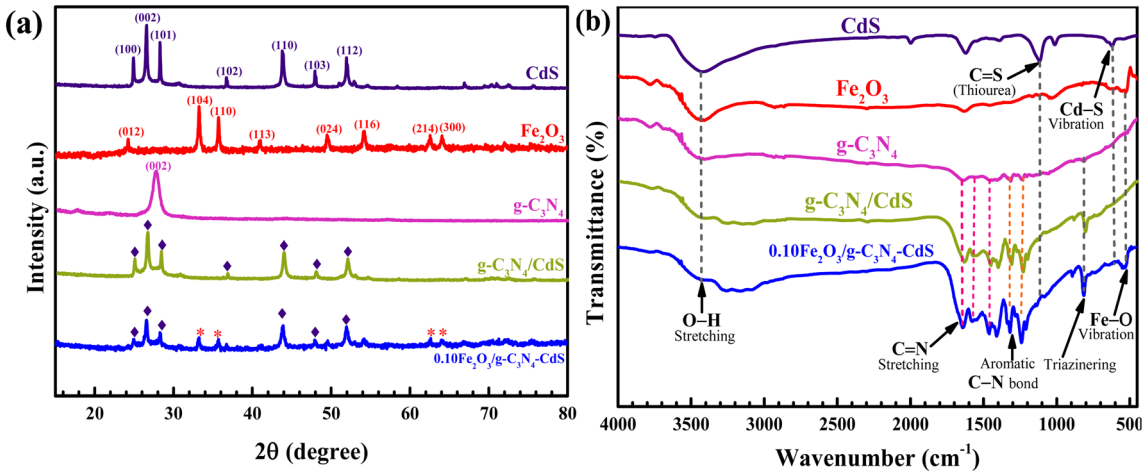

Fig. 1 XRD patterns (a) and FT-IR spectra (b) of all the prepared photocatalysts.

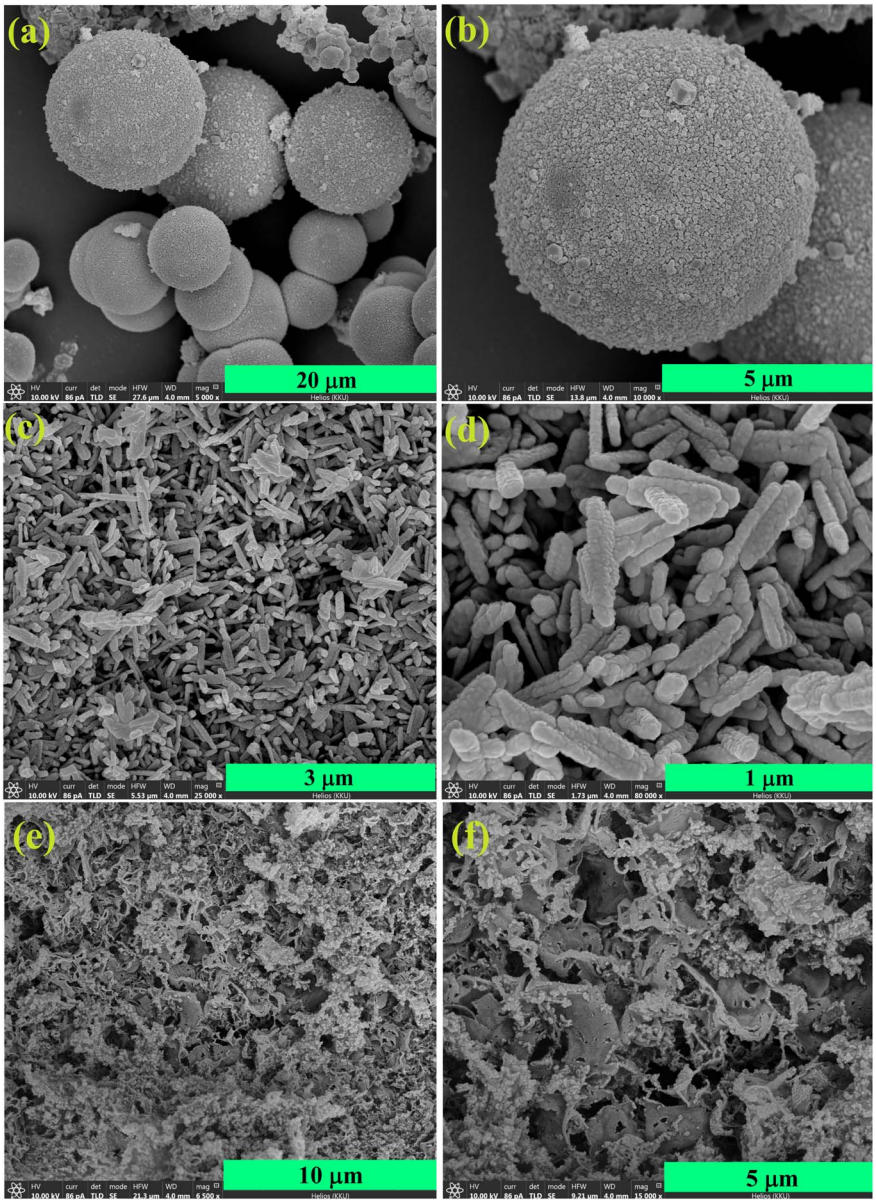

Fig. 2 FE-SEM micrographs of the pristine photocatalysts, namely CdS (a and b), Fe_2O_3 (c and d), and g-C_3N_4 (e and f).

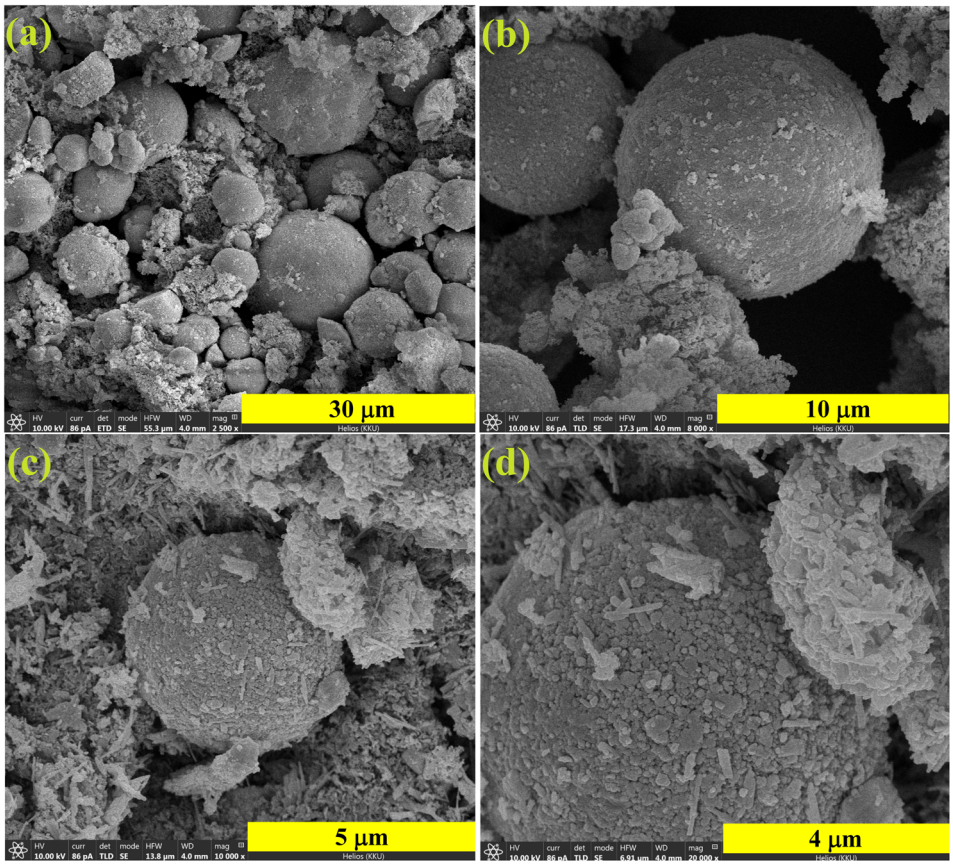

Fig. 3 FE-SEM micrographs of the binary g-C_3N_4/CdS photocatalyst (a and b) and the ternary 0.10Fe_2O_3/g-C_3N_4/CdS photocatalyst (c and d).

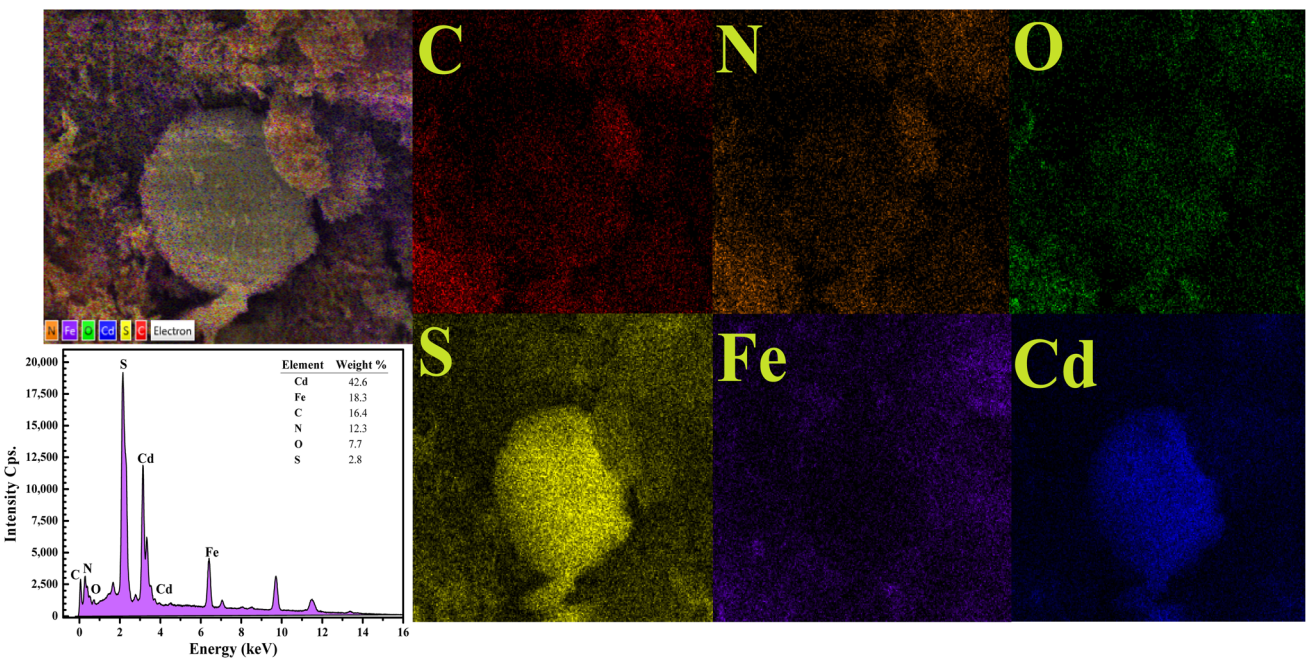

Fig. 4 The EDS spectrum, SEM image of the mapped area, and the EDS elementary mapping confirm the presence of Cd, S, Fe, O, C, and N elements in the 0.10Fe_2O_3/g-C_3N_4/CdS photocatalyst.

indicated the C=S stretching vibration in the thiourea complex.[2] Fe_2O_3 displayed a vibrational band at 535 cm^{-1}, confirming the Fe–O bond.[12] In the case of the bare g-C_3N_4 photocatalyst, the peak at 820 cm^{-1} was assigned to the vibration mode due to the presence of the triazine ring. Besides, three bands at 1655 cm^{-1}, 1587 cm^{-1} and 1473 cm^{-1} were assigned to the C=N vibration of g-C_3N_4.[12] The bands at 1337 and 1260 cm^{-1} were attributed to the aromatic C–N vibrational frequencies.[12] g-C_3N_4/CdS displayed vibrational bands from CdS and g-C_3N_4. The ternary 0.10Fe_2O_3/g-C_3N_4/CdS photocatalyst provided the additional bands of Fe_2O_3, in comparison to those detected in the g-C_3N_4/CdS binary photocatalyst. The information from the vibrational spectra confirmed the successful generation of the ternary 0.10Fe_2O_3/g-C_3N_4/CdS photocatalyst.

The morphological structure of the prepared photocatalyst was investigated by SEM. The micrographs of CdS (Fig. 2a and b) revealed the spherical morphology of about 9 μm. The SEM images of Fe_2O_3 (Fig. 2c and d) provided a rod-like structure with a size of about 0.10 × 0.37 μm. As shown in Fig. 2e and f, the pristine g-C_3N_4 photocatalyst revealed the wrinkles together with the sheet-like morphology.[12] The SEM images of binary g-C_3N_4/CdS showed the uniform destruction of g-C_3N_4 on spherical CdS (Fig. 3a and b). The 0.10Fe_2O_3/g-C_3N_4/CdS catalyst (Fig. 3c and d) displayed the co-existence of three components, namely, CdS, g-C_3N_4 and Fe_2O_3, indicating the successful generation of the ternary photocatalyst.

The EDX method was used to determine the amount of the elements in 0.10Fe_2O_3/g-C_3N_4/CdS, as displayed in Fig. 4. Six elements, namely cadmium, sulfur, carbon, nitrogen, iron and oxygen, were found. In addition, the EDX mapping confirms the uniform distribution of Cd, S, C, N, Fe and O in the synthesized photocatalyst.[2,6,12] The results strongly indicate the finding of CdS, g-C_3N_4 and Fe_2O_3 in the ternary photocatalyst.

The presence of all components in the binary and ternary photocatalysts was verified by TEM and HR-TEM, as shown in Fig. S1.[26,35,36] In the case of the binary g-C_3N_4/CdS photocatalyst (Fig. S1a and b), the HR-TEM images indicated the lattice fringes with '*d*' spacings of 0.31 nm and 0.32 nm, corresponding to the (101) plane of CdS and the (002) plane of g-C_3N_4, respectively. In the case of the ternary photocatalyst, the identity of all the three components is presented in Fig. S1c and d, confirming their co-existence in the ternary heterojunction. It is seen that lattice fringes with '*d*' spacings of 0.20 nm, 0.25 nm and 0.32 nm are assigned to the finding of the (110) plane of CdS, the (110) plane of Fe_2O_3, and the (002) plane of g-C_3N_4, respectively.

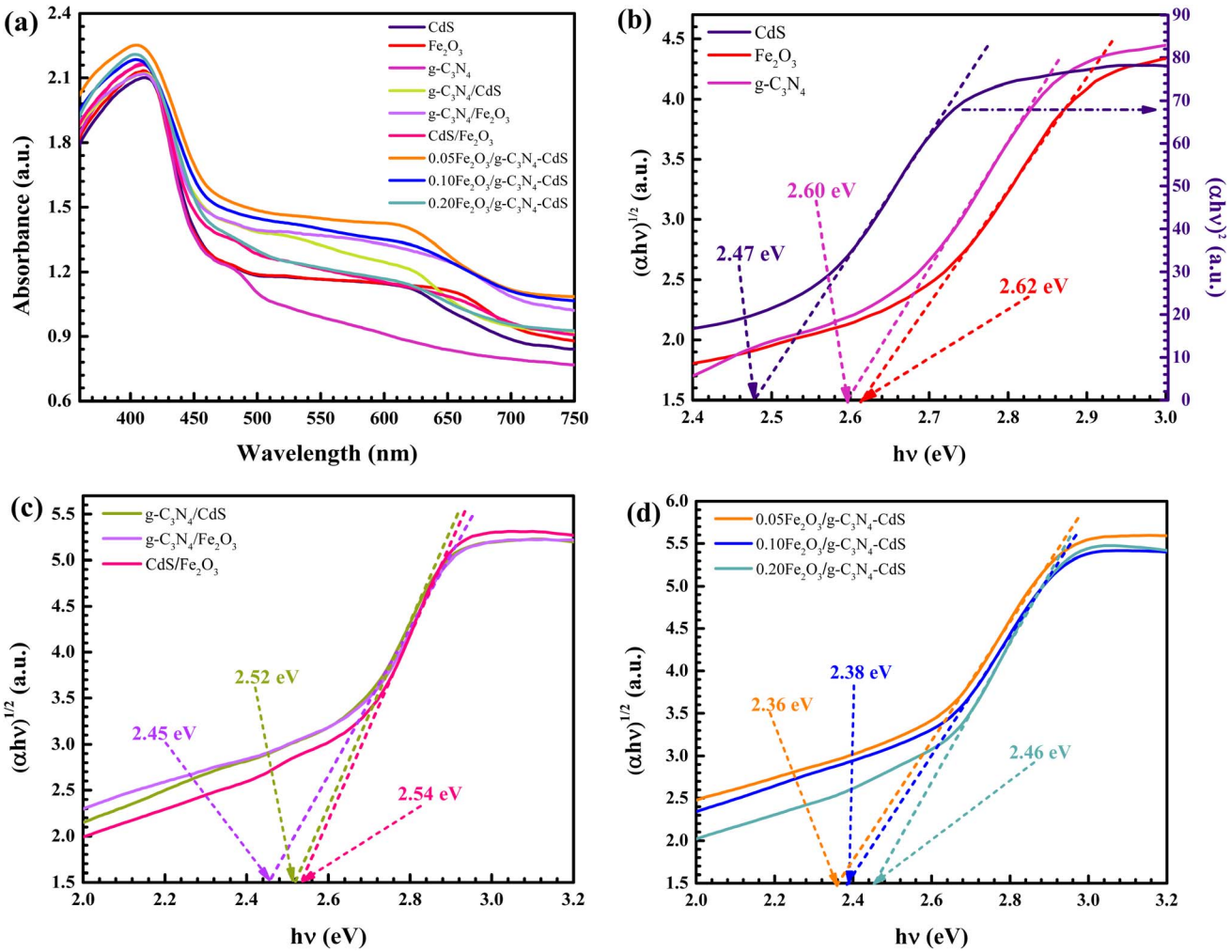

Fig. 5 Diffused reflectance spectra (a) and Tauc plots for the determination of the band gap (b–d) of the synthesized photocatalysts.

The optical spectra of the catalysts were measured. As shown in Fig. 5a, the absorption edges of CdS, g-C_3N_4, and Fe_2O_3 were at 502 nm, 477 nm and 473 nm, respectively. The band energy was calculated using the Kubelka–Munk equation after extrapolation to the *x*-axis.[8,11,12] The band energy of 2.47 eV was obtained from CdS, while the values of about 2.60 eV and 2.62 eV were reported from g-C_3N_4 and Fe_2O_3, respectively (Fig. 5b). The binary photocatalysts (Fig. 5c) showed enhanced absorbance within the visible light region, with a band gap of 2.45–2.54 eV. After careful determination, the 0.10Fe_2O_3/g-C_3N_4/CdS photocatalyst showed a band gap of 2.38 eV (light absorption ≈ 521 nm), as clearly shown in Fig. 5d. The results from optical spectra demonstrate the red shift of photo-absorption toward the visible light region, in comparison to those of the single components.[8,11,12] This indicates an increase in visible light absorption after the generation of the 0.10Fe_2O_3/g-C_3N_4/CdS photocatalyst. Thus, the improvement in the photocatalytic performance will be found in the ternary photocatalyst. To sum up, the 0.10Fe_2O_3/g-C_3N_4/CdS photocatalyst improved the photo-absorption over the visible light region, which, in turn, eventually led to an enhancement in the resulting photoactivity.

In theory, the charge separation speed and charge transport rate are very important in terms of determining the resulting photoactivity of the sample.[8,11,12] It is accepted that the fluorescence intensity implies the electron–hole pair recombination efficiency. The lowest fluorescence intensity infers the highest charge separation speed. This will end up with the maximum photocatalytic activity.[2,6] Fig. 6a–c show the fluorescence spectra of the prepared catalysts detected at $\lambda_{excitation}$ of 355 nm, 400 nm and 440 nm. It is clearly seen that the fluorescence intensity of the 0.10Fe_2O_3/g-C_3N_4/CdS photocatalyst was the lowest among all the prepared samples implying the slowest recombination of electron–hole pairs. In principle, the ternary 0.10Fe_2O_3/g-C_3N_4/CdS photocatalyst is expected to provide the greatest photocatalytic performance, compared to the bare components, the binary photocatalysts and the ternary photocatalysts with 0.05 and 0.20 wt% of Fe_2O_3. The details based on the photodegradation of the TC drug and CR dye will be discussed later.

Fig. S2 shows the time-resolved photoluminescence (TRPL) decay curves and the lifetimes of the prepared catalysts (Table S1). The ternary 0.10Fe_2O_3/g-C_3N_4/CdS photocatalyst displayed the fastest decay time, compared to the bare Fe_2O_3, he pristine g-C_3N_4 and binary –C_3N_4/CdS photocatalysts. The average lifetimes (τ_{Ave}) for the Fe_2O_3, g-C_3N_4, CdS, g-C_3N_4/CdS and 0.10Fe_2O_3/g-C_3N_4/CdS photocatalysts were found to be 6.40, 5.48, 5.26, 4.89 and 4.78 ns, respectively. The TRPL fitting curve parameters of the prepared

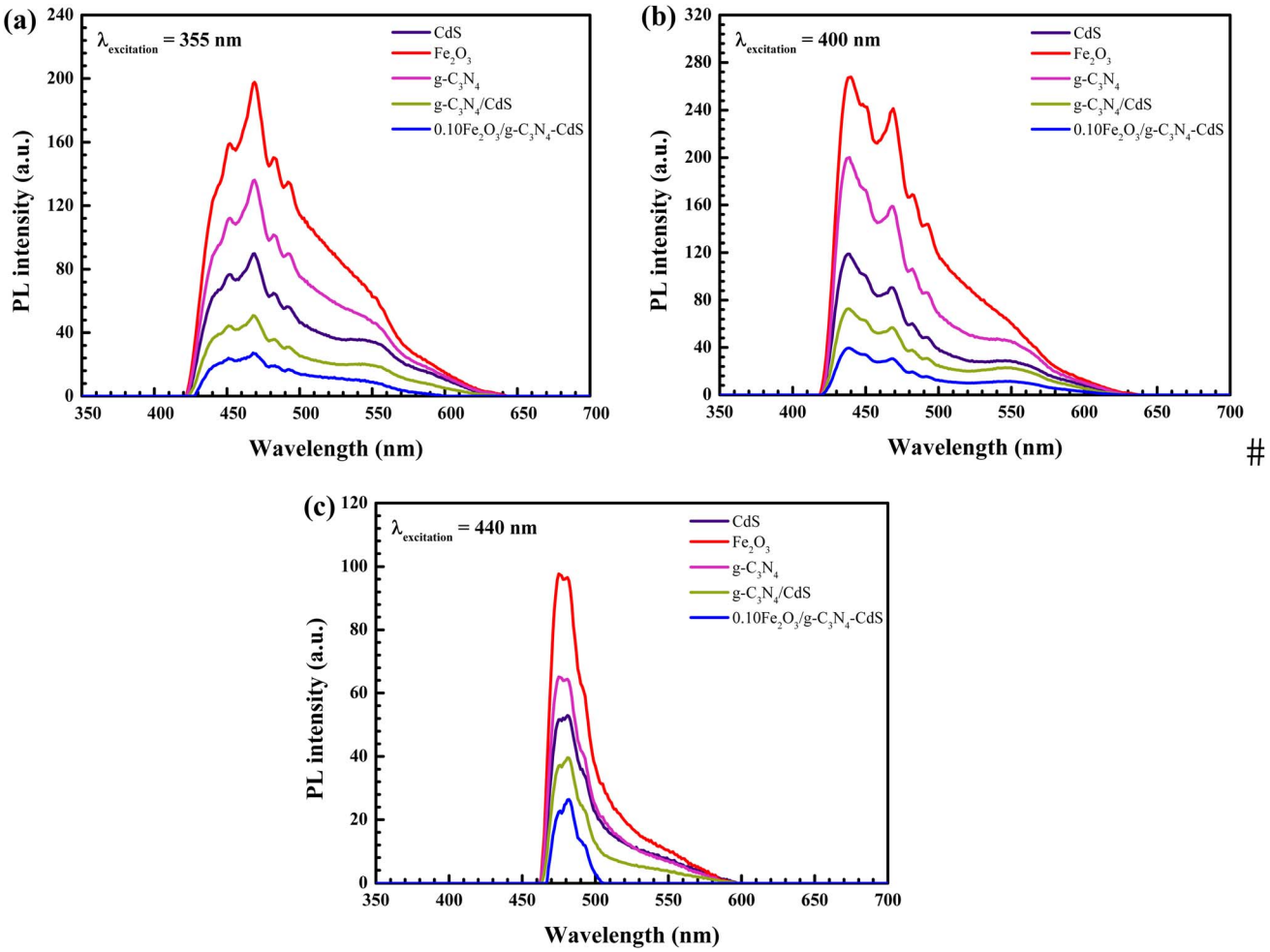

Fig. 6 PL spectra of the synthesized photocatalysts using $\lambda_{excitation}$ of 355 nm (a), 400 nm (b), and 440 nm (c).

photocatalysts are shown in Table S1. A dramatic reduction in the average lifetime of the ternary 0.10Fe_2O_3/g-C_3N_4/CdS photocatalyst indicates a drastic decrease in the charge transfer time after the generation of the ternary catalyst, demonstrating that some new non-radiative processes for charge carriers genuinely exist in the 0.10Fe_2O_3/g-C_3N_4/CdS photocatalyst.[26]

A photoelectrochemical method was used to investigate the carrier transport properties. The electrochemical investigation was performed using the linear sweep voltammetric (LSV) technique.[12] The plots of LSV scans (Fig. 7a) indicated that the 0.10Fe_2O_3/g-C_3N_4/CdS photocatalyst showed the maximum photocurrent density, compared to the bare components. The result indicates the greatest content of total charge carriers detected in the ternary heterojunction. The prepared 0.10Fe_2O_3/g-C_3N_4/CdS photocatalyst exhibited the greatest carrier separation speed and this will finally result in the maximum photocatalytic activity reported for this ternary heterostructure photocatalyst.

The charge separation of the catalyst was roughly compared after analyzing the results from the electrochemical impedance spectroscopic (EIS) method.[12] It is extensively accepted that the lowest arc radius indicates the lowest charge-transfer resistance.[12] From Fig. 7b, the 0.10Fe_2O_3/g-C_3N_4/CdS photocatalyst showed the smallest arc radius, indicating the lowest resistance of charge transfer. Obviously, the result showed that the creation of the ternary catalyst caused improved charge separation speed, which will finally lead to an astonishing increment in the final photoactivity. All in all, the results from fluorescence spectra correlate well with the plots from the electrochemical experiment, confirming the promising performance of the ternary catalyst.

To examine the mechanism concerning the improved photocatalytic efficiency detected in the 0.10Fe_2O_3/g-C_3N_4/CdS photocatalyst, the Mott–Schottky plots were constructed, so that the band structures of all catalysts can be drawn (see Fig. 7c and d).[12] The values of the flat band potential (V_{FB}) of CdS, Fe_2O_3 and g-C_3N_4 were at about −0.40, 0.45 and −1.02 eV, respectively. Therefore, the V_{CB} level of CdS, Fe_2O_3 and g-C_3N_4 was at about −0.40, 0.45 and −1.02 eV, respectively. Previously (Fig. 5b), the band gap energy of CdS, Fe_2O_3, and g-C_3N_4 was 2.47 eV, 2.62 eV and 2.60 eV, respectively. Accordingly, the V_{VB} levels of 2.07, 3.07 and 1.58 eV were calculated, respectively, from the CdS, Fe_2O_3 and g-C_3N_4 photocatalysts. The calculated CB and VB potentials of these bare components are shown again in Fig. 14. Accordingly, the proposed mechanism based on the photodegradation of the pollutant will also be discussed.

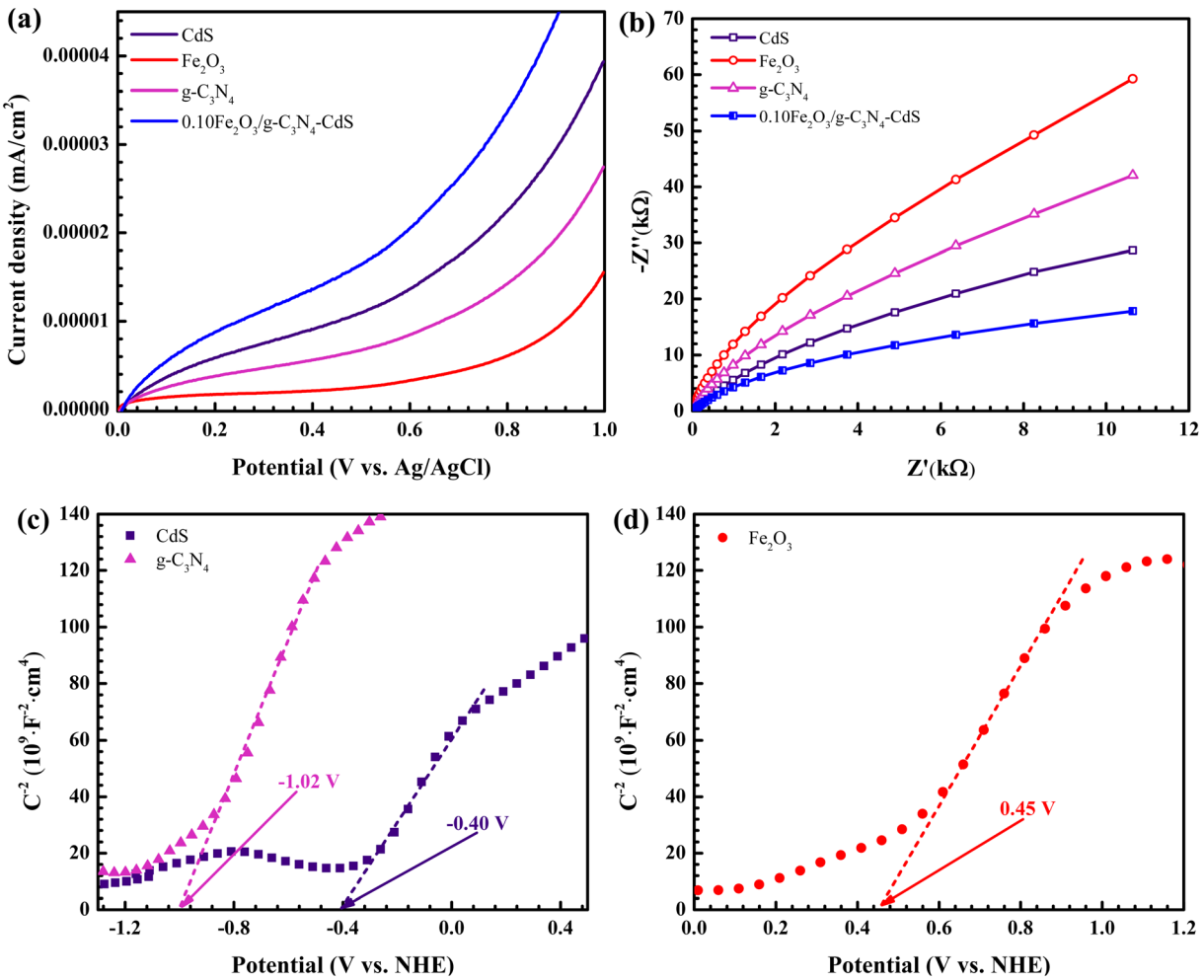

Fig. 7 Linear sweep voltammetry (LSV) scans plots (a), electrochemical impedance spectroscopy (EIS) Nyquist plots (b) and Mott–Schottky plots (c and d) of the samples using a frequency of 30 Hz in 0.5 M Na_2SO_4.

3.2 Removal of the TC antibiotic

The degradation of TC was investigated using the simulated UV-vis light (an LED lamp, 15 W) and the natural sunlight irradiation. The effect of TC content, catalyst amount, and solution pH on the resulting photocatalytic activity was fully examined.[8,11]

3.2.1 Removal of the TC drug under UV-vis light. The photocatalytic efficiency of all the prepared catalysts was studied. As shown in Fig. 8a, the self-degradation of TC (from photolysis process) is negligible. Only 17% TC removal was achieved *via* the adsorption process in the dark. Obviously, the 0.10Fe_2O_3/g-C_3N_4/CdS photocatalyst revealed an enhanced photocatalytic performance of 84% (Fig. 8b). The photocatalytic efficiency was about

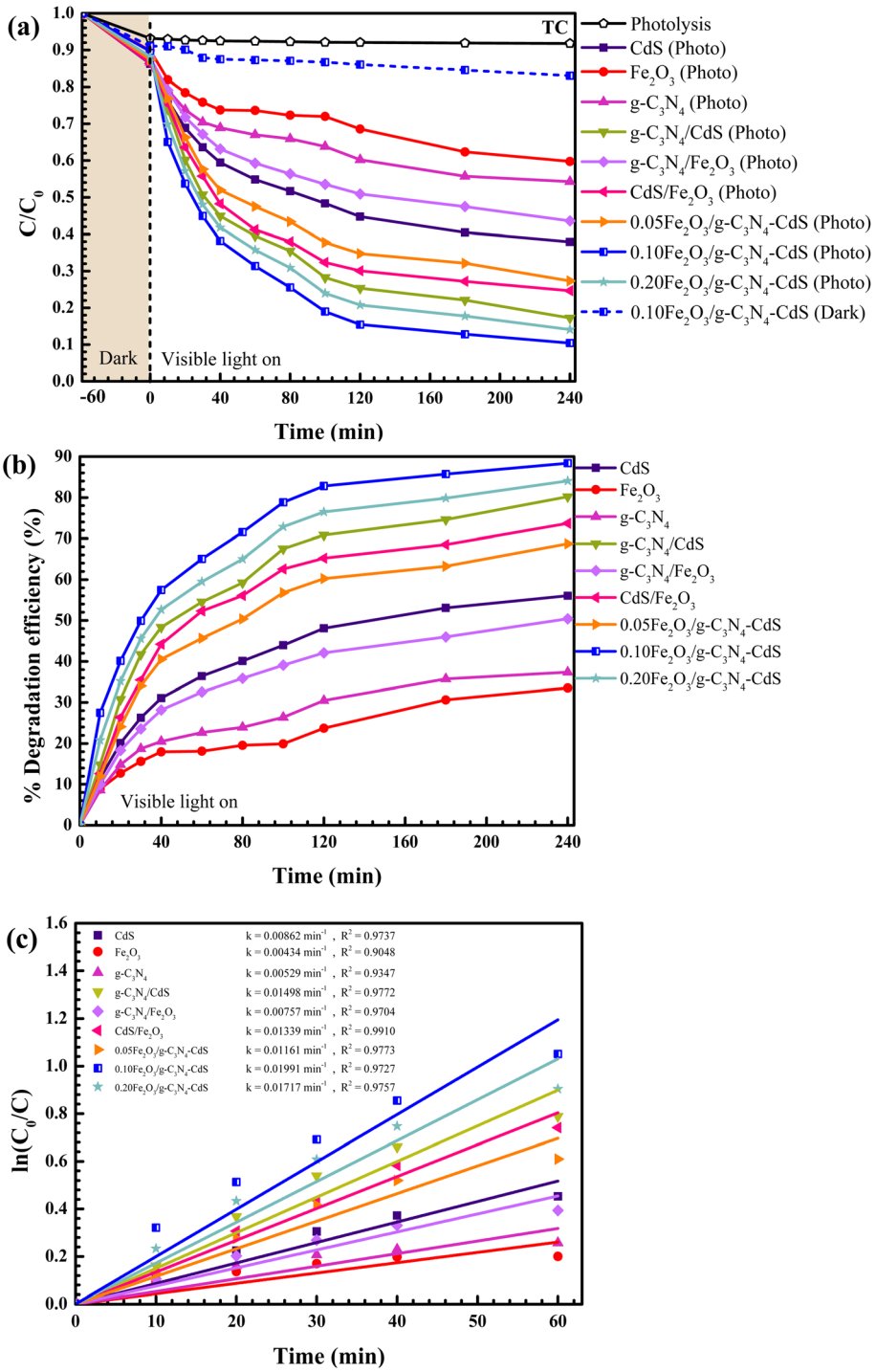

Fig. 8 Plots of TC concentration *vs.* time (a), corresponding photodegradation efficiency (b) and plots of ln(C_0/C) *vs.* time for the determination of the rate constants (c).

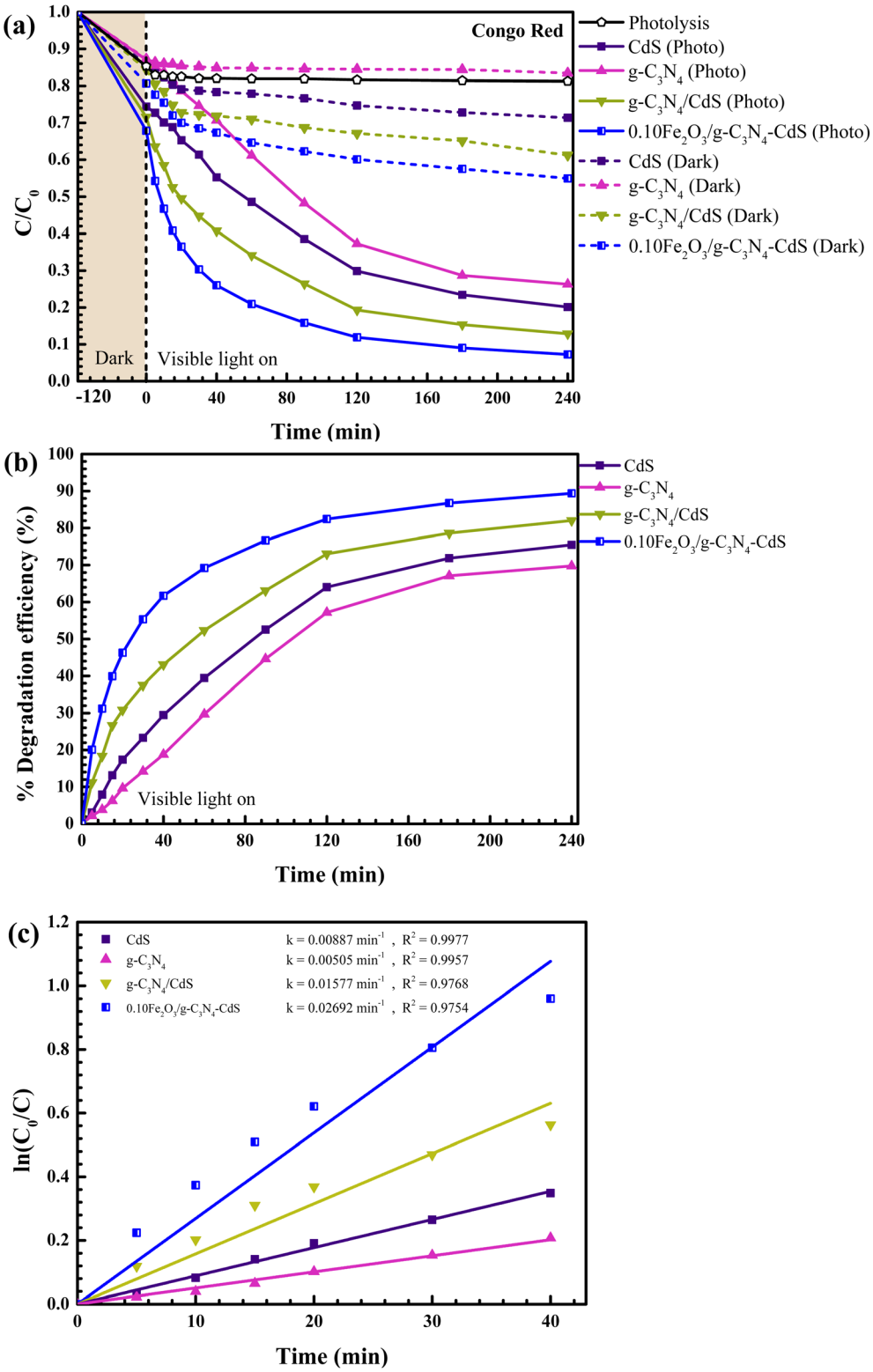

Fig. 9 Plots of Congo red concentration *vs.* time (a), corresponding photodegradation efficiency (b) and plots of $\ln(C_0/C)$ *vs.* time for the determination of rate constants (c).

1.5 times, 2.5 times and 2.3 times greater than that of the pristine CdS, Fe_2O_3 and g-C_3N_4 photocatalysts, respectively. As shown in Fig. 8c, the ternary photocatalyst provides a maximum rate constant of 0.0172 min^{-1}. It is noted that the photocatalytic efficiency and the degradation rate detected from the 0.10Fe_2O_3/g-C_3N_4/CdS photocatalyst were greater than those observed from

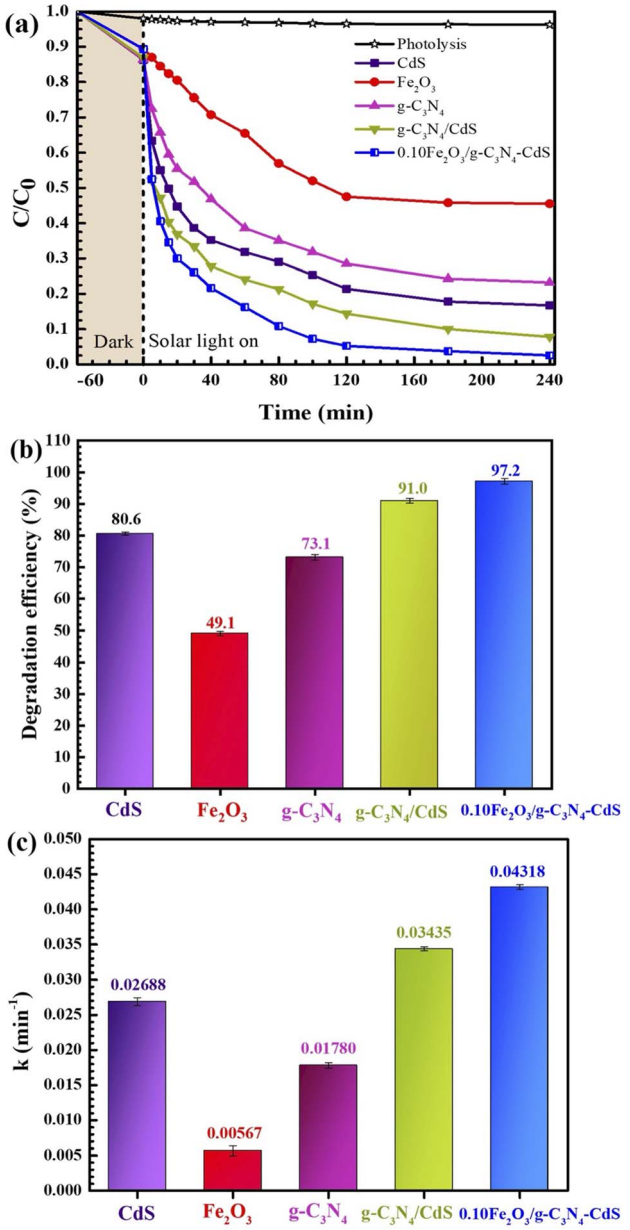

Fig. 10 Lowering of the TC concentration with time under natural sunlight (a), the corresponding photodegradation efficiency (b) and the rate constants for TC degradation (c).

the bare components and the binary photocatalysts. This is attributed to the enhancement of charge separation speed after the creation of the ternary catalyst.

Furthermore, the photodegradation test was performed by monitoring the removal of Congo red dye, as shown in Fig. 9. Lowering of the dye concentration can be clearly seen in Fig. 9a. It can be observed that self-degradation of Congo red (the photolysis of the dye) is negligible. Besides, about 40% adsorption of the dye (in the dark) can be reported. As shown in Fig. 9b, the $0.10Fe_2O_3/g\text{-}C_3N_4/CdS$ photocatalyst displayed the maximum photoactivity of 90% after photo-illumination. The degradation efficiency is higher, approximately 1.2 times, 1.3 times and 1.1 times than that of the bare CdS, pristine $g\text{-}C_3N_4$ and binary $g\text{-}C_3N_4/CdS$ photocatalysts, respectively. From Fig. 9c, the ternary photocatalyst provides the maximum rate constant of 0.0269 min^{-1}. The final degradation performance and the degradation rate detected from the $0.10Fe_2O_3/g\text{-}C_3N_4/CdS$ photocatalyst are the maximum among all the prepared photocatalysts.

3.2.2 Removal of TC under natural solar light. After solar light irradiation, the prepared catalyst displayed its improved photocatalytic efficiency toward TC removal, as shown in Fig. 10. The highest photoactivity is observed from the $0.10Fe_2O_3/g\text{-}C_3N_4/CdS$ photocatalyst. The efficiency reached 97% after 4 h of sunlight illumination (Fig. 10b). Fig. 10c shows the plot of $\ln(C_0/C)$ *vs.* time. The highest first-order rate constant of 0.0432 min^{-1} was determined for the ternary catalyst. In summary, the detoxification of TC antibiotic under UV-vis light and under natural solar light (Fig. 10) confirmed the astonishing enhancement in photoactivity after the generation of the ternary catalyst.[11,12]

3.2.3 Effect of some parameters on the photocatalytic activity. The effect of some parameters including TC concentration, catalyst loading, and solution pH on the resulting photoactivity was fully examined. As shown in Fig. 11a, an increase in TC amount results in a decrease in photoactivity. The enhancement in the drug concentration results in an increment in photo-absorption by the antibiotic rather than the prepared catalyst. This will finally end up with lowering of the photon flux entering the catalyst.[11,12] Thus, a decrease in the photocatalytic performance was found. Utilizing a TC solution of either 5 or 10 ppm revealed a similar photocatalytic efficiency within 4 h. Altogether, 10 ppm of TC was fixed.

The important role of the catalyst content on the photoactivity was also examined (Fig. 11b). As demonstrated, the addition of catalysts results in an improvement in the photoactivity. This is ascribed to the high amount of the antibiotic adsorbed on the catalyst surface. Additionally, the improved photoactivity is ascribed to the increase in catalyst content in the area of photo-exposure.[8] However, a decrease in the photoactivity was detected after using 75 mg photocatalyst. Therefore, the catalyst amount was fixed at 50 mg.

The solution pH is an important parameter involved in the degradation efficiency. The effect of solution pH (range from 3 to 11) on the photoactivity was examined (Fig. 11c). The natural solution pH of TC is around 7. The TC drug shows pK_a values of 3.3, 7.8 and 9.6.[11,12] A much reduction in the photoactivity at pH $\approx$ 3 is assigned to the dissolution of the catalyst.[8,11,12] The solution pH of around 7 provided the maximum photocatalytic efficiency after 4 h. Adjusting the solution pH is not necessary.

3.2.4 Trapping method. The trapping experiment was performed to investigate the degradation mechanism of the antibiotic.[11,12] The effect of numerous quenchers on TC degradation can be clearly seen (Fig. 12). It is well accepted that $K_2Cr_2O_7$, isopropanol (IPA), sodium azide (NaN_3) and the EDTA-2Na were used as the scavengers of electrons, $^{\bullet}OH$, singlet oxygen atoms, and photo-created holes, respectively. Besides, KI was utilized as the quencher of holes and surface hydroxyls. As shown in Fig. 12a and b, a dramatic decrease in the photocatalytic performance to 29.7% was detected after the incorporation of

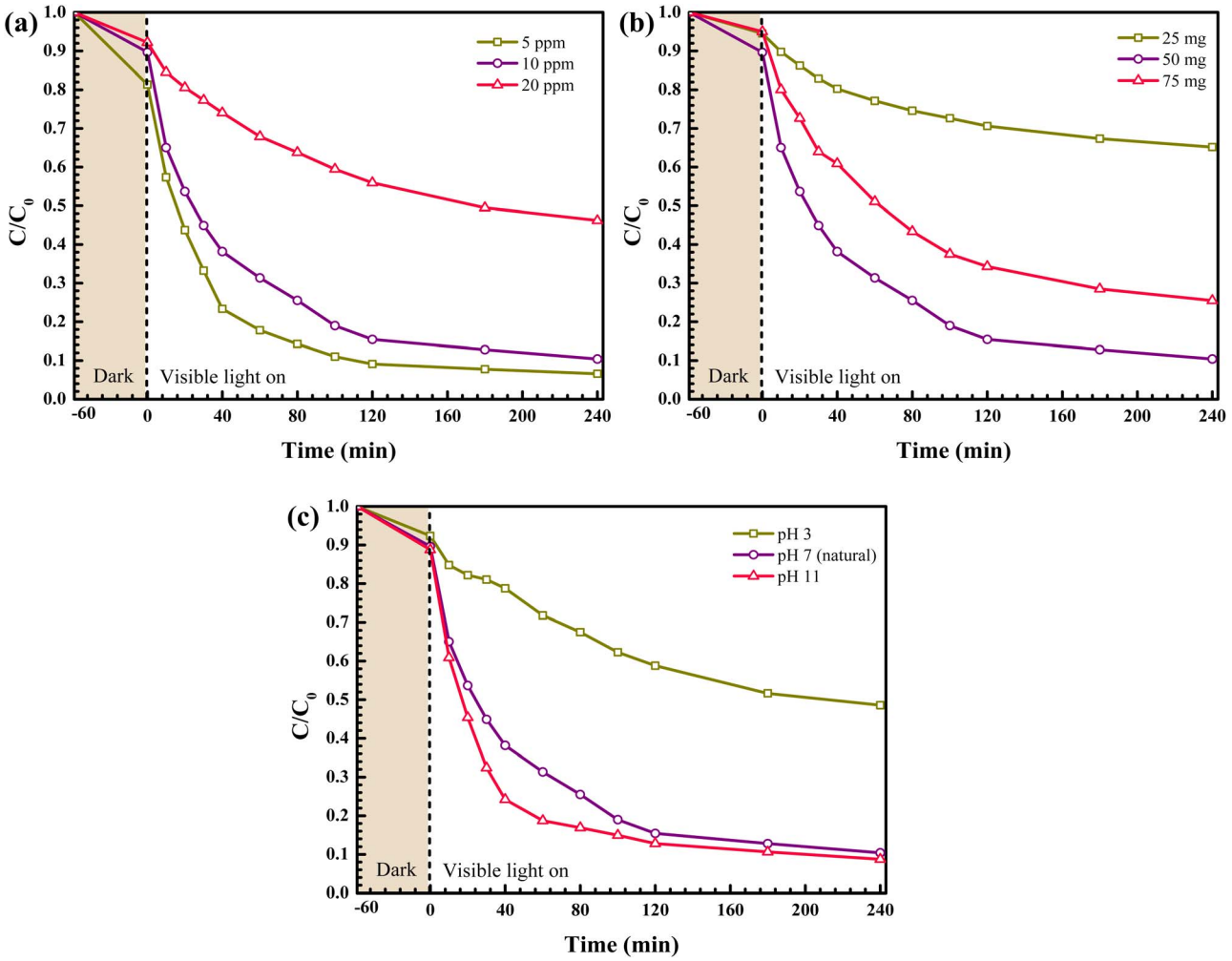

Fig. 11 The effect of the initial concentration (a), catalyst content (b) and initial solution pH (c) on the photodegradation of TC antibiotic.

EDTA-2Na, indicating the major role of the photo-created holes in TC removal.[11,12] From Fig. 12c, the rate constant (k) achieved after the addition of EDTA-2Na is 7.7×10^{-4} min^{-1}, while that detected from the no scavenger process (in an absence of any quencher) is 0.0199 min^{-1}. Interestingly, around 25.8 times lowering of the rate constant was observed, indicating the huge role of the photo-created holes in TC detoxification.

Besides, the generation of $OH^{\bullet}$, after light exposure, was investigated *via* the terephthalic acid (TPA) probe technique.[12] In theory, TPA reacts with the hydroxyl radicals to create the 2-hydroxy terephthalic acid (with the detection of fluorescence intensity), known as hydroxy-TPA. Fig. 12d reveals the increase in fluorescence intensity (425 nm) with time for the ternary photocatalyst, indicating the formation of the hydroxy-TPA. The PL spectra strongly confirmed the role of hydroxyl radicals in the detoxification of TC.

Furthermore, the study involved in the approximation of the $OH^{\bullet}$ amount after 60 min and 240 min of light illumination was conducted. As shown in Fig. 13, the fluorescence signal, due to the creation of hydroxy-TPA, at about 60 min and 240 min reveals the same development of plot of fluorescence signal *vs.* time. The ternary photocatalyst showed the maximum PL intensity, compared to the bare CdS and the binary g-C_3N_4/CdS photocatalyst, confirming the generation of the highest content of $OH^{\bullet}$. This finding is in good agreement with the maximum degradation rate detected in the ternary catalyst.[12]

After photo-irradiation, the generation of holes and electrons can be observed. The electron–hole pairs will then react with the other species to generate the novel reactive species playing a key role in the removal of the antibiotic. After that, the drug molecule was removed and will end up with the formation of CO_2, H_2O and some degraded compounds.[8,11,12]

The energy regarding the CB and VB levels of CdS, g-C_3N_4 and Fe_2O_3 was investigated, based on the results from the electro-chemical technique (Fig. 7) and the band gap values from the optical spectra (Fig. 5). The energy levels (Fig. 14) suggested a *Z*-scheme mechanism.[12,35,36,55] The creation of the ternary catalyst facilitated the excellent separation of carriers. Thus, a considerable enhancement in the photoactivity can be obtained. The construction of the ternary heterojunctions offers advantages over the creation of just binary heterojunctions. The

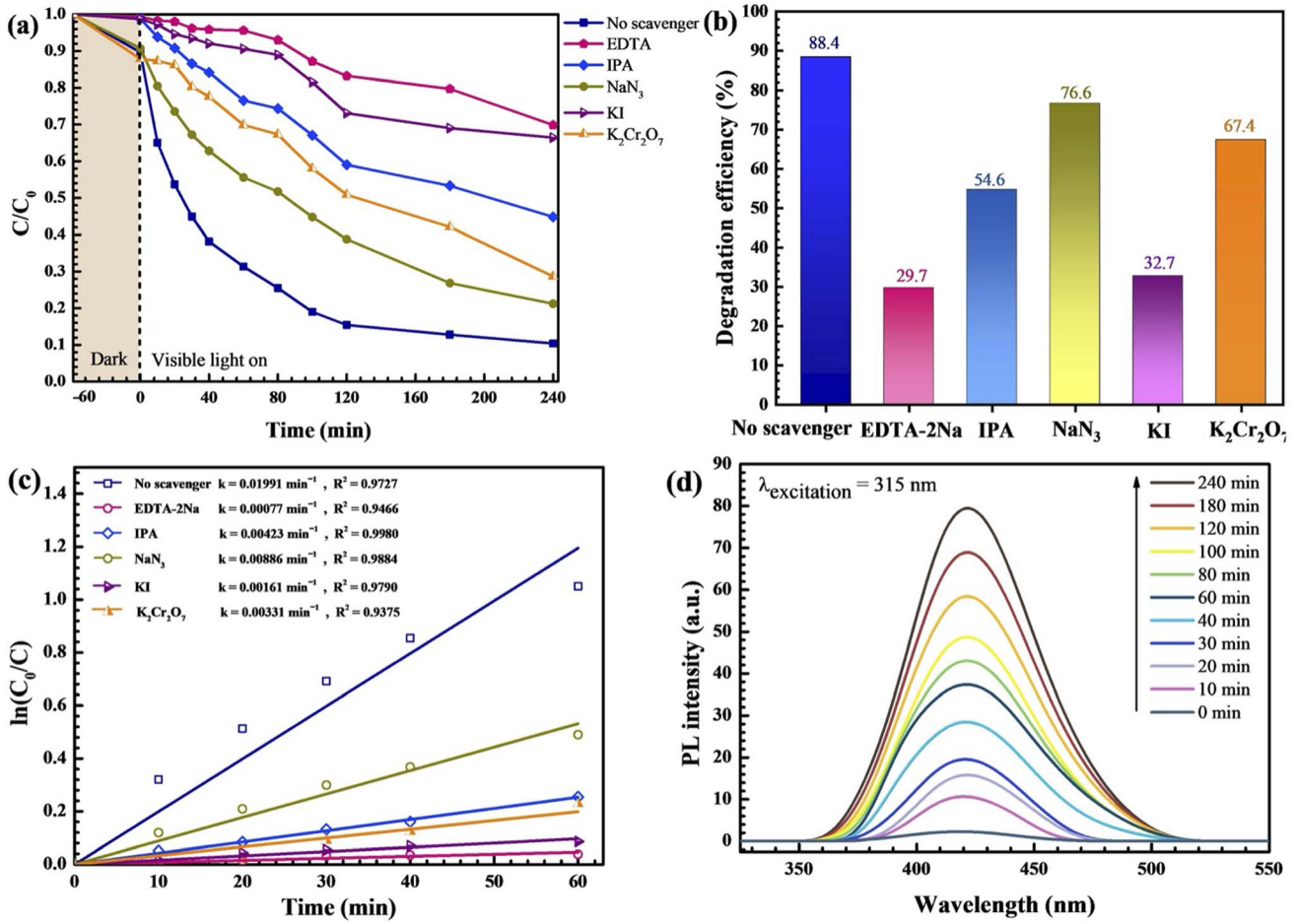

Fig. 12 Lowering of C/C_0 with time (a), the corresponding photodegradation efficiency (b), the rate constants regarding TC degradation with the addition of various scavengers (c), and the hydroxyl radical trapping PL spectra of the solution after photoillumination of the 0.10Fe_2O_3/g-C_3N_4-CdS photocatalyst (d).

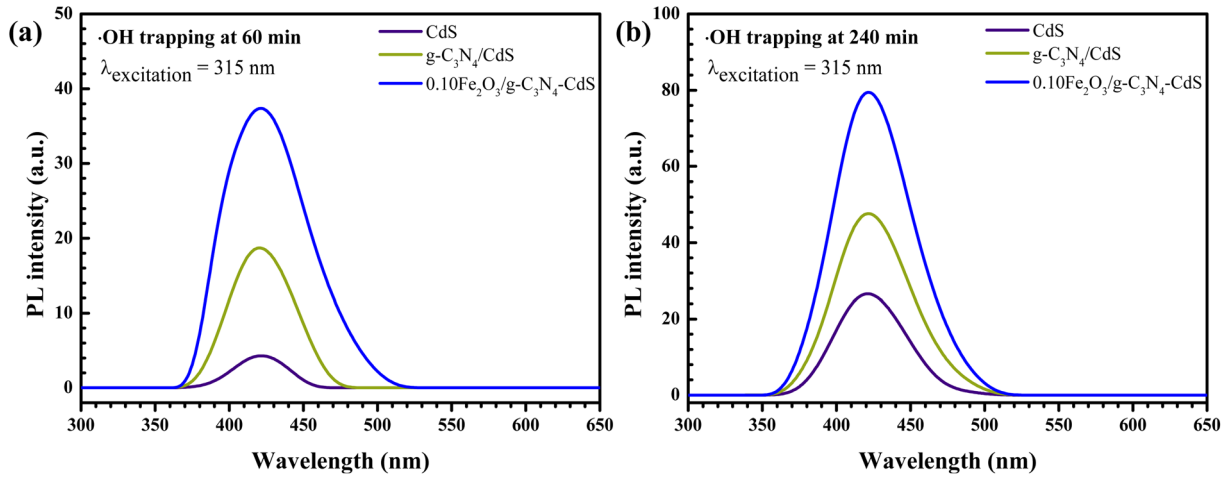

Fig. 13 Hydroxyl radical trapping PL spectra of CdS, g-C_3N_4/CdS and 0.10Fe_2O_3/g-C_3N_4/CdS photocatalysts after 60 min (a) and 240 min (b) of photoirradiation.

merits include prolonged lifetime of electron–hole pairs and enhancement of visible light absorption.[26] In addition, ternary heterojunctions based on CdS, Fe_2O_3, and g-C_3N_4 have been previously reported in the literature.[35,36] The details of TC degradation by the ternary photocatalysts can be summarized as follows:[8,11,12]

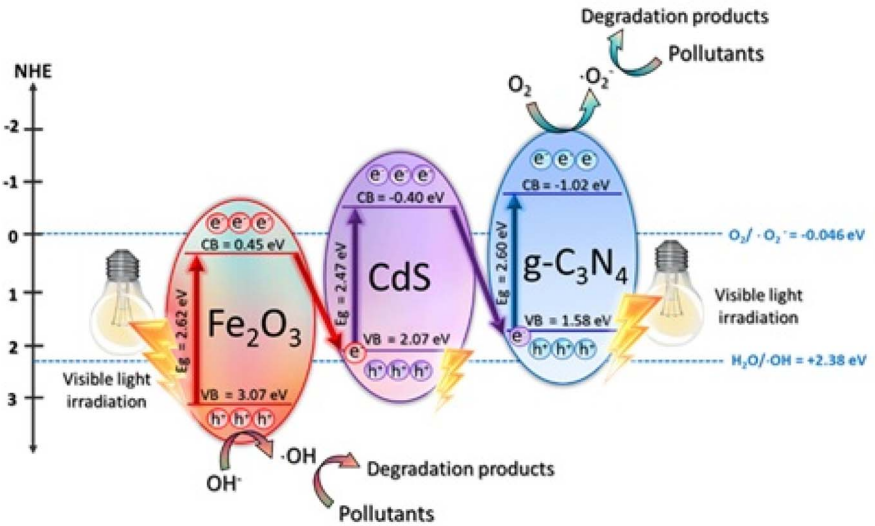

Fig. 14 The proposed *Z*-scheme mechanism found in the Fe_2O_3/g-C_3N_4/CdS heterojunction toward the degradation of the TC antibiotic.

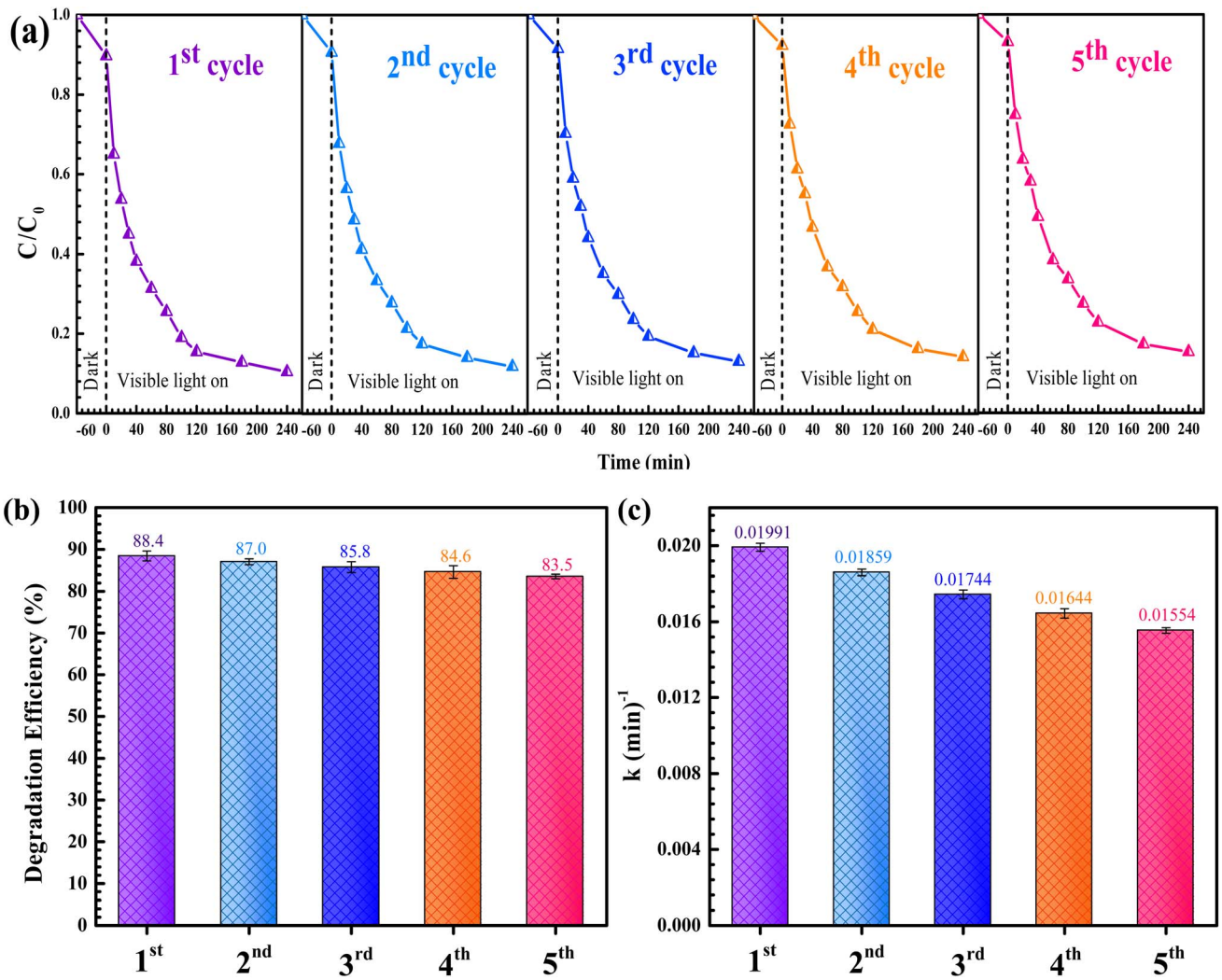

Fig. 15 Reusability of the 0.10Fe_2O_3/g-C_3N_4/CdS photocatalyst toward TC degradation (a), the corresponding photodegradation efficiency (b) and the rate constants (c) detected after five cycles of use.

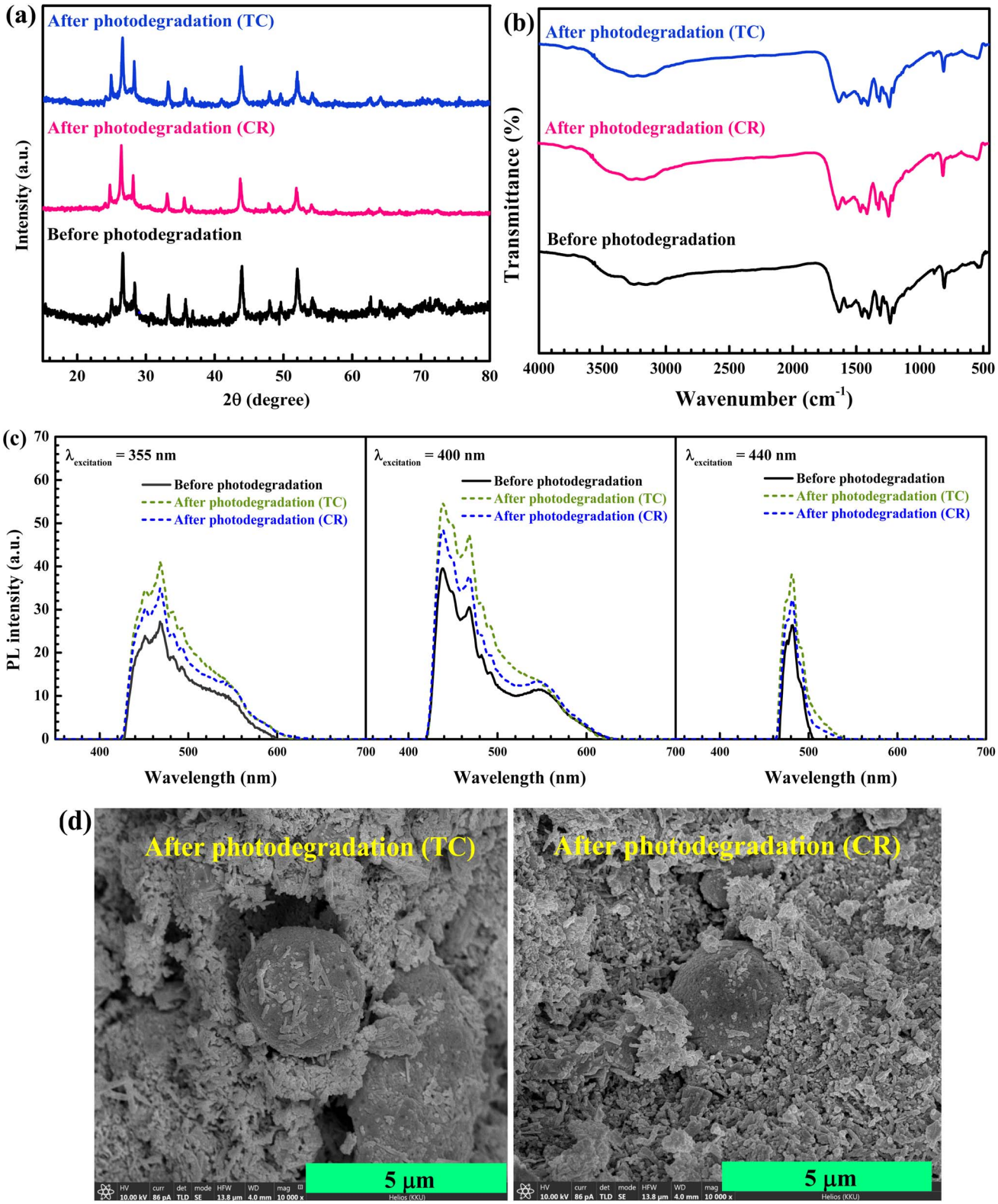

Fig. 16 XRD patterns (a), vibrational spectra (b), PL spectra (c) and SEM images of the 0.10Fe_2O_3/g-C_3N_4/CdS photocatalyst after the degradation of TC antibiotic and CR dye (d).

Table 1 TC detoxification in the presence of various photocatalysts

Photocatalyst	Conc.	Catalyst loading	Light source	Power (W)	Time (min)	Degradation (%)	Ref.
Capped-ZnO	10 mg L^{-1}	50 mg	UV	135	80	99	8
ZnO/BiOBr	30 mg L^{-1}	40 mg	Ultrasonic	—	75	87	9
ZnO/BiOI	10 mg L^{-1}	20 mg	Visible	—	160	90	10
Fe_3O_4/ZnO	10 mg L^{-1}	50 mg	UV	135	20	100	11
Fe_2O_3/ZnO/g-C_3N_4	10 mg L^{-1}	50 mg	Sunlight	—	240	100	12
Fe_2O_3/ZnO/g-C_3N_4	10 mg L^{-1}	50 mg	UV	135	240	97	12
Fe_3O_4/BiOCl/BiOBr	40 mg L^{-1}	20 mg	Visible	(Xenon, 300 W)	80	85	13
Fe_3O_4/BiOCl/BiOI	40 mg L^{-1}	20 mg	Visible	(Xenon, 300 W)	80	89	14
Fe_2O_3/g-C_3N_4/CdS	10 mg L^{-1}	50 mg	UV	135	240	84	This work
Fe_2O_3/g-C_3N_4/CdS	10 mg L^{-1}	50 mg	Sunlight	—	240	97	This work

$$\text{Photocatalyst} + \text{light} \rightarrow \text{photocatalyst} + e^- + h^+ \quad (4)$$

$$e^- + O_2 \rightarrow {}^{\bullet}O_2^- \quad (5)$$

$${}^{\bullet}O_2^- + 2H_2O + e^- \rightarrow 2{}^{\bullet}OH + 2OH^- \quad (6)$$

$$h^+ + TC \rightarrow \text{degraded compounds} \quad (7)$$

$${}^{\bullet}OH + TC \rightarrow \text{degraded compounds} \quad (8)$$

The proposed pathways of TC degradation have been reported in previous works.[44,56,57] Numerous major routes were presented.[44,56,57] The degraded products were indicated using the data achieved from the LC-MS experiment. The final products, including water and carbon dioxide, with no toxicity were obtained.[44,56,57]

Reusability is a crucial factor affecting the application of the synthesized catalyst.[8,11,12,58,59] Thus, the cycling ability of the prepared catalyst was studied for five cycles (Fig. 15a). As shown in Fig. 15b and c, the prepared catalyst still exhibits its enhanced efficiency, with the promising rate constant for five cycles. The stability of the catalyst was also confirmed. The XRD diffractograms (Fig. 16a), FT-IR spectra (Fig. 16b), and PL spectra (Fig. 16c) of the fresh and used catalysts are more or less the same. In addition, the SEM images (Fig. 16d) confirmed that the ternary photocatalyst still revealed promising photoactivity with a similar morphological structure after use for the removal of TC.

The removal of TC by the synthesized catalysts was summarized.[8–14] In this study, we investigated the TC removal by Fe_2O_3/g-C_3N_4/CdS. The photoactivities of this ternary catalyst and the other catalysts reported in previous works are compared in Table 1. The UV-active ZnO photocatalyst reached a photocatalytic efficiency of 99%.[8] The binary photocatalysts, namely, ZnO/BiOBr and ZnO/BiOI provided 87–90% detoxification of TC.[9,10] Interestingly, magnetic Fe_3O_4/ZnO revealed complete degradation of the TC drug (100% removal).[11] Ternary Fe_2O_3/ZnO/g-C_3N_4 revealed the performance up to 100%.[12] Meanwhile, the ternary BiOCl-based heterostructure showed an efficiency of 85–89%.[13,14] In this work, the prepared ternary photocatalyst showed 84% removal of TC under UV-vis light and 97% under natural solar light irradiation. Altogether, the enhanced photocatalytic performance of the prepared Fe_2O_3/g-C_3N_4/CdS photocatalyst for efficient detoxification of TC was demonstrated.

After the photodegradation of organic pollutants, the possibility of photo-corrosion of the prepared Fe_2O_3/g-C_3N_4/CdS photocatalyst was also studied.[60–62] The amount of the released Cd^{2+} ions from the pristine CdS photocatalyst and the ternary Fe_2O_3/g-C_3N_4/CdS photocatalyst was investigated by the inductively coupled plasma (ICP) technique, as shown in Fig. S3. It is seen that about 30.8 mg L^{-1} and 4.0 mg L^{-1} of Cd^{2+} were found in the solution after the photodegradation of TC antibiotic for 240 min, using CdS and Fe_2O_3/g-C_3N_4/CdS, respectively. It should be noted that the amount of Cd^{2+} released from the ternary Fe_2O_3/g-C_3N_4/CdS photocatalyst was much lower than that obtained from the bare CdS photocatalyst. The results strongly indicated that the anti-photocorrosion property of the photocatalyst was successfully achieved after the generation of the ternary heterojunction.[60] Altogether, the prepared Fe_2O_3/g-C_3N_4/CdS photocatalyst exhibited not only promising sunlight-driven photodegradation efficiency but also very low photo-corrosion levels in comparison to that of the pristine CdS photocatalyst.

4. Conclusions

The ultrasonication technique was used for the synthesis of the solar-light-driven 0.10Fe_2O_3/g-C_3N_4/CdS catalyst. The co-existence of CdS, g-C_3N_4 and Fe_2O_3 was confirmed. Under UV-vis light, the synthesized photocatalyst revealed 84% degradation of TC within 4 h. Interestingly, 97% detoxification of TC was achieved under sunlight. The ternary photocatalyst showed an astonishing enhancement in photocatalytic performance, compared to all the prepared photocatalysts, owing to the increase in carrier separation speed after the formation of the ternary catalyst. The photo-generated holes play a crucial role in the degradation of the harmful drug. The promising cyclability of the catalyst was also demonstrated for five cycles. This research provides a facile route to create ternary heterojunctions for TC degradation under the abundant natural sunlight.

Conflicts of interest

There are no conflicts to declare.

Data availability

The data that support the findings of this study are available from the corresponding author, S. Nanan, on request.

Supplementary information: TEM and HR-TEM images, TRPL spectra, and Cd^{2+} detected in the TC solution in the presence of the prepared photocatalysts. See DOI: https://doi.org/10.1039/d5ra04984a.

Acknowledgements

This work was supported by Research and Graduate Studies, Khon Kaen University (Research Program, fiscal year 2024). We would also like to thank the partial financial support from the Center of Excellence for Innovation in Chemistry (PERCH-CIC).

References

1 T. Senasu, N. Ruengchai, S. Khamdon, N. Lorwanishpaisarn and S. Nanan, Hydrothermal Synthesis of Cadmium Sulfide Photocatalyst for Detoxification of Azo Dyes and Ofloxacin Antibiotic in Wastewater, *Molecules*, 2022, **27**, 7944, DOI: 10.3390/molecules27227944.

2 T. Senasu, K. Hemavibool and S. Nanan, Hydrothermally grown CdS nanoparticles for photodegradation of anionic azo dyes under UV-visible light irradiation, *RSC Adv.*, 2018, **8**, 22592–22605, DOI: 10.1039/c8ra02061b.

3 T. Sansenya, N. Masri, T. Chankhanittha, T. Senasu, J. Piriyanon, S. Mukdasai and S. Nanan, Hydrothermal synthesis of ZnO photocatalyst for detoxification of anionic azo dyes and antibiotic, *J. Phys. Chem. Solids*, 2022, **160**, 110353, DOI: 10.1016/j.jpcs.2021.110353.

4 T. Chankhanittha, V. Somaudon, J. Watcharakitti and S. Nanan, Solar light-driven photocatalyst based on bismuth molybdate (Bi_4MoO_9) for detoxification of anionic azo dyes in wastewater, *J. Mater. Sci.: Mater. Electron.*, 2021, **32**, 1977–1991, DOI: 10.1007/s10854-020-04965-5.

5 T. Chankhanittha, J. Watcharakitti and S. Nanan, PVP-assisted synthesis of rod-like ZnO photocatalyst for photodegradation of reactive red (RR141) and Congo red (CR) azo dyes, *J. Mater. Sci.: Mater. Electron.*, 2019, **30**, 17804–17819, DOI: 10.1007/s10854-019-02132-z.

6 T. Senasu and S. Nanan, Photocatalytic performance of CdS nanomaterials for photodegradation of organic azo dyes under artificial visible light and natural solar light irradiation, *J. Mater. Sci.: Mater. Electron.*, 2017, **28**, 17421–17441, DOI: 10.1007/s10854-017-7676-x.

7 T. Chankhanittha, V. Somaudon, J. Watcharakitti, V. Piyavarakorn and S. Nanan, Performance of solvothermally grown Bi2MoO6 photocatalyst toward degradation of organic azo dyes and fluoroquinolone antibiotics, *Mater. Lett.*, 2020, **258**, 126764, DOI: 10.1016/j.matlet.2019.126764.

8 P. Thangsan, K. Wannakan and S. Nanan, Biosynthesis of ZnO using *Senna siamea* leaf extract for photodegradation of tetracycline antibiotic and azo dye in wastewater, *OpenNano*, 2024, **16**, 100202, DOI: 10.1016/j.onano.2024.100202.

9 Z. Ma, Y. He, X. Li, C. Zhou and L. Deng, Ultrasonic-assisted efficient degradation of tetracycline over ZnO/BiOBr heterojunctions: Synergistic effect and role of oxidative species, *Mater. Res. Bull.*, 2022, **146**, 111591, DOI: 10.1016/j.materresbull.2021.111591.

10 X. Chen, S. Du, L. Gao, K. Shao, Z. Li and B. Liu, A hydrangea-like nitrogen-doped ZnO/BiOI nanocomposite for photocatalytic degradation of tetracycline hydrochloride, *Nanoscale Adv.*, 2023, **5**, 1936–1942, DOI: 10.1039/d2na00896c.

11 A. Panchakeaw, S. Nonthing, R. Dulyasucharit and S. Nanan, Improved photocatalytic activity of magnetically separable Fe_3O_4/ZnO photocatalyst for complete sunlight-active removal of tetracycline antibiotic, *Chem. Phys. Lett.*, 2025, **862**, 100253, DOI: 10.1016/j.cplett.2025.141868.

12 K. Wannakan, S. Nonthing, A. Panchakeaw and S. Nanan, Ternary Fe_2O_3/g-C_3N_4/ZnO photocatalyst for complete sunlight-driven degradation of tetracycline antibiotic, *Diamond Relat. Mater.*, 2025, **155**, 112316, DOI: 10.1016/j.diamond.2025.112316.

13 J. Dang, J. Zhang, Y. Shen, L. Wang, F. Guo, Y. Li and W. Guan, Fabrication of magnetically recyclable Fe_3O_4/BiOCl/BiOBr nanocomposite with Z-scheme heterojunction for high-efficiency photocatalytic degradation of tetracycline, *Mater. Sci. Semicond. Process.*, 2023, **158**, 107371, DOI: 10.1016/j.mssp.2023.107371.

14 J. Dang, J. Guo, L. Wang, F. Guo, W. Shi, Y. Li and W. Guan, Construction of Z-scheme Fe_3O_4/BiOCl/BiOI heterojunction with superior recyclability for improved photocatalytic activity towards tetracycline degradation, *J. Alloys Compd.*, 2022, **893**, 162251, DOI: 10.1016/j.jallcom.2021.162251.

15 M. Song, J. He, Y. Liu, Y. Wu and Y. Su, Degradation of tetracycline by photocatalysis combined with activated peroxymonsulfate over S-scheme $BiVO_4/Fe_2O_3$ heterojunction, *J. Environ. Chem. Eng.*, 2024, **12**, 113300, DOI: 10.1016/j.jece.2024.113300.

16 H. Fang, C. Zhou, S. Xu, J. Shi, Y. Hu and G. Liu, S-scheme photocatalyst Mo_2C/α-Fe_2O_3 with vacant oxygen for highly efficient tetracycline degradation in peroxymonosulfate-mediated photocatalytic system, *J. Alloys Compd.*, 2023, **958**, 170547, DOI: 10.1016/j.jallcom.2023.170547.

17 D. Meng, J. Hou, L. Wang, X. Hu, D. Gao and Q. Guo, Rational construction of α-Fe_2O_3/g-C_3N_4 heterojunction for effective photo-Fenton-like degradation of tetracycline, *Mater. Res. Bull.*, 2023, **168**, 112454, DOI: 10.1016/j.materresbull.2023.112454.

18 R. Selvaraj, D. Prabhu, P. S. Kumar, G. Rangasamy, G. Murugesan, M. Rajesh, L. C. Goveas, T. Varadavenkatesan, A. Samanth, R. Balakrishnaraja and R. Vinayagam, Adsorptive removal of tetracycline from aqueous solutions using magnetic Fe_2O_3/activated carbon prepared from Cynometra ramiflora fruit waste, *Chemosphere*, 2023, **310**, 136892, DOI: 10.1016/j.chemosphere.2022.136892.

19 A. Alahabadi, N. Shomoossi, F. Riahimanesh and M. Salari, Development of AC/ZnO/Fe_2O_3 for efficiently adsorptive removal of Tetracycline from water environment: isotherm, kinetic and thermodynamic studies and adsorption mechanism, *Biomass Convers. Biorefin.*, 2024, **14**, 17499–17517, DOI: 10.1007/s13399-023-03875-w.

20 H. Sun, G. Liang, B. Chen, J. Jia and H. Jing, A novel ZnO/$Fe3^+$-doped Bi_2WO_6 photocatalyst with triple synergistic effect for solar-driven tetracycline degradation, *RSC Adv.*, 2025, **15**, 12689–12697, DOI: 10.1039/d5ra01899d.

21 R. Zhang, J. Dong, L. Li, J. Zhao, M. Ji, B. Wang, J. Xia and H. Li, Low concentration of peroxymonosulfate coupled with visible light triggers oxygen reactive species generation over constructed $Bi_{25}FeO_{40}$/BiOCl Z-scheme heterojunction for various tetracycline antibiotics removal, *J. Colloid Interface Sci.*, 2024, **665**, 825–837, DOI: 10.1016/j.jcis.2024.03.138.

22 T. Chankhanittha and S. Nanan, Visible-light-driven photocatalytic degradation of ofloxacin (OFL) antibiotic and Rhodamine B (RhB) dye by solvothermally grown ZnO/Bi_2MoO_6 heterojunction, *J. Colloid Interface Sci.*, 2021, **582**, 412–427, DOI: 10.1016/j.jcis.2020.08.061.

23 J. Piriyanon, P. Takhai, S. Patta, T. Chankhanittha, T. Senasu, S. Nijpanich, S. Juabrum, N. Chanlek and S. Nanan, Performance of sunlight responsive WO_3/AgBr heterojunction photocatalyst toward degradation of Rhodamine B dye and ofloxacin antibiotic, *Opt. Mater.*, 2021, **121**, 111573, DOI: 10.1016/j.optmat.2021.111573.

24 T. Narenuch, T. Senasu, T. Chankhanittha and S. Nanan, Sunlight-active BiOI photocatalyst as an efficient adsorbent for the removal of organic dyes and antibiotics from aqueous solutions, *Molecules*, 2021, **26**, 5624, DOI: 10.3390/molecules26185624.

25 J. Piriyanon, T. Chankhanittha, S. Youngme, K. Hemavibool, S. Nijpanich, S. Juabrum, N. Chanlek and S. Nanan, Fabrication of MoS_2/Ag_3PO_4 S-scheme photocatalyst for visible-light-active degradation of organic dye and antibiotic in wastewater, *J. Mater. Sci.: Mater. Electron.*, 2021, **32**, 19798–19819, DOI: 10.1007/s10854-021-06504-2.

26 T. Chankhanittha, B. Johnson, R. J. Bushby, T. Butburee, P. Khemthong and S. Nanan, One-pot hydrothermal synthesis of g-C_3N_4/BiOBr/Bi_2MoO_6 as a Z-scheme heterojunction for efficient photocatalytic degradation of ciprofloxacin (CIP) antibiotic and Rhodamine B (RhB) dye, *J. Alloys Compd.*, 2024, **1008**, 176764, DOI: 10.1016/j.jallcom.2024.176764.

27 S. Das and Y. H. Ahn, Synthesis and application of CdS nanorods for LED-based photocatalytic degradation of tetracycline antibiotic, *Chemosphere*, 2022, **291**, 132870, DOI: 10.1016/j.chemosphere.2021.132870.

28 H. Ye, J. Du, X. Ding, G. Cai, Y. Peng, Y. Fu and G. Zuo, Cage-like magnetic CdS/MgFe2O4 S-scheme heterojunction material for photocatalytic decomposition of tetracycline hydrochloride, *J. Mater. Res.*, 2024, **39**, 1562–1575, DOI: 10.1557/s43578-024-01331-7.

29 T. Luo, X. Sun, D. Ma, G. Wang, F. Yang, Y. Zhang, J. Huang, H. Zhang, J. Wang and F. Peng, Fabrication of TiO2/CdS Heterostructure by Soluble Solid-State Titanium-oxo-Clusters for Fast Photocatalytic Degradation of Tetracycline, *J. Phys. Chem. C*, 2023, **127**, 1372–1380, DOI: 10.1021/acs.jpcc.2c06101.

30 H. Yu, J. Zhang, R. Zhai, C. Gao, Y. Zhang, C. Tian and Q. Ma, Magnetic biochar-doped g-C3N4/Fe2O3 S-scheme heterojunction with enhanced photocatalytic degradation of tetracycline by addition of persulfate, *Carbon*, 2024, **230**, 119681, DOI: 10.1016/j.carbon.2024.119681.

31 Z. Zhu, N. Zhou, Y. Li, X. Zhang and L. Zhang, Step scheme Fe2O3/S doped g-C3N4 heterojunction photocatalysts for photo-fenton norfloxacin and tetracycline degradation, *Mater. Sci. Semicond. Process.*, 2023, **160**, 107423, DOI: 10.1016/j.mssp.2023.107423.

32 D. Hou, L. Han, H. Yang, Z. Yang, Y. Liu, S. Huang, Z. Peng, T. Lu, X. Si, X. Liu, J. Li and J. Wang, Calcium-doped CaCO3/g-C3N4 with cyano groups for efficient photo-fenton degradation of tetracycline, *J. Water Proc. Eng.*, 2025, **75**, 108083, DOI: 10.1016/j.jwpe.2025.108083.

33 Y. M. Alrababah and C. K. Sheng, Wurtzite CdS ratio tunability on α-Fe2O3/CdS synergistic heterostructure for enhanced UV-induced photocatalytic decomposition of rhodamine 6G dye pollutant, *Alex. Eng. J.*, 2024, **100**, 300–311, DOI: 10.1016/j.aej.2024.05.050.

34 W. Wang, G. Wei, Z. Fan, L. Zhang, J. Gu and F. Gao, Novel RM based S-scheme heterojunction Bi2WO6/Fe2O3 as an effective activator for peroxydisulfate in the degradation of tetracycline hydrochloride under visible light: Preparation, application, and degradation mechanism, *J. Environ. Chem. Eng.*, 2025, **13**, 116192, DOI: 10.1016/j.jece.2025.116192.

35 M. S. Athar, M. Danish and M. Muneer, Fabrication of visible light-responsive dual Z-Scheme (α-Fe2O3/CdS/g-C3N4) ternary nanocomposites for enhanced photocatalytic performance and adsorption study in aqueous suspension, *J. Environ. Chem. Eng.*, 2021, **9**, 105754, DOI: 10.1016/j.jece.2021.105754.

36 C. Yavuz and S. Erten-Ela, Solar light-responsive α-Fe2O3/CdS/g-C3N4 ternary photocatalyst for photocatalytic hydrogen production and photodegradation of methylene blue, *J. Alloys Compd.*, 2022, **908**, 164584, DOI: 10.1016/j.jallcom.2022.164584.

37 W. Zhou, A. Shui, M. Cai and H. Yu, One-pot synthesis of Bi/Bi_2WO_6/ZnO ternary heterojunction with oxygen vacancies for photodegradation driven by visible light, *Opt. Mater.*, 2025, **166**, 117169, DOI: 10.1016/j.optmat.2025.117169.

38 L. Wang, X. Wang, X. Xu, F. Wu and Y. Ge, Construction of ZnO quantum dots anchored in oxygen-doped g-C_3N_4: A novel Z-type heterojunction with boosting photocatalytic performance for tetracycline degradation, *J. Mol. Struct.*, 2025, **1328**, 141382, DOI: 10.1016/j.molstruc.2025.141382.

39 X. M. Zhang, C. Xu, C. Bin Yu, K. Yang, K. Q. Lu, W. Y. Huang and Z. Q. Liu, Oxygen vacancy defect engineering in MoO_2/Mo-doped BiOCl Ohmic junctions for enhanced

photocatalytic antibiotic elimination, *J. Alloys Compd.*, 2024, **1005**, 176220, DOI: 10.1016/j.jallcom.2024.176220.

40 Z. xu Wang, X. wen Zhu, C. hong Chen, M. Yang, H. Yu, X. ting Dong and Y. Yang, Bi-QDs modified β-Bi_2O_3/BiOCl ternary bismuth series photocatalyst and its photocatalytic properties, *J. Solid State Chem.*, 2025, **345**, 125225, DOI: 10.1016/j.jssc.2025.125225.

41 J. Luo, L. Wu, D. Liu, Y. Chen, Q. Lv and H. Deng, Preparation of S-scheme heterojunction photocatalyst Y_2O_3/BiOCl and visible light degradation of ofloxacin: Photocatalytic mechanism, DFT calculation, degradation pathway, and toxicity evaluation, *J. Alloys Compd.*, 2025, **1010**, 177888, DOI: 10.1016/j.jallcom.2024.177888.

42 A. Saadati, A. Habibi-Yangjeh and A. Khataee, S-scheme QDs-sized photocatalyst fabricated through combination of TiO_{2-x} with gray BiOCl for efficient removal of organic pollutants upon visible light, *J. Alloys Compd.*, 2025, **1010**, 177621, DOI: 10.1016/j.jallcom.2024.177621.

43 A. R. Amani-Ghadim, Y. Bahadori, A. Dabirnia, S. Ahmadian-Kordasht, S. Arefi-Oskoui, A. Khataee and S. Sattari, Embedding CdTe@CdS QDs into the C3N5 nanosheets with enhanced activity for visible-light-driven photocatalytic degradation of methylene blue and tetracycline, *Inorg. Chem. Commun.*, 2025, **178**, 114553, DOI: 10.1016/j.inoche.2025.114553.

44 Y. Shi, R. Zhao, W. Yang, Q. Bu, L. Yang and J. Tang, Interface-coupled supramolecular self-assembly 2D Z-scheme TiO2/g-C3N4 heterojunction for efficient degradation of tetracycline under visible light, *J. Alloys Compd.*, 2025, **1018**, 179252, DOI: 10.1016/j.jallcom.2025.179252.

45 Z. Mahdavi, A. A. Amooey, S. Ghasemi and M. Varmaziar, Degradation of tetracycline by magnetic BiOI/S-doped g-C3N4/NiFe2O4 nanocomposite through visible-light photocatalysis process, *Diamond Relat. Mater.*, 2025, **155**, 112306, DOI: 10.1016/j.diamond.2025.112306.

46 M. Abdoli, Z. Ciğeroğlu and Y. Açıkbaş, Eco-friendly synthesis of ZnO/g-C3N4 using Salix aegyptiaca extract: A high-performance photocatalyst for tetracycline degradation under visible light, response surface methodology, *J. Mol. Struct.*, 2025, **1332**, 141719, DOI: 10.1016/j.molstruc.2025.141719.

47 S. Shuang, Z. Xie and Z. Zhang, Enhanced photocatalytic properties of CdS nanoparticles decorated α-Fe2O3 nanopillar arrays under visible light, *J. Colloid Interface Sci.*, 2017, **494**, 107–113, DOI: 10.1016/j.jcis.2017.01.086.

48 J. Y. Wang, J. Xu, W. Shao and C. J. Qian, Photodeposition of Fe2O3 on CdS with high dispersion for efficient decomposing tetracycline, *Chem. Phys. Lett.*, 2022, **786**, 139170, DOI: 10.1016/j.cplett.2021.139170.

49 H. Feng, S. Feng, N. Tang, S. Zhang, X. Zhang and B. Liu, Fabrication of TiO2/Fe2O3/CdS systems: effects of Fe2O3and CdS content on superior photocatalytic activity, *RSC Adv.*, 2021, **11**, 10300–10308, DOI: 10.1039/d1ra00195g.

50 K. Sharma, A. Sudhaik Sonu, R. Kumar, V. H. Nguyen, Q. Van Le, T. Ahamad, S. Thakur, S. Kaya, L. H. Nguyen, P. Raizada and P. Singh, Advanced photo-Fenton assisted degradation of tetracycline antibiotics using α-Fe2O3/CdS/SiO2 based S-scheme photocatalyst, *J. Water Proc. Eng.*, 2024, **59**, 105011, DOI: 10.1016/j.jwpe.2024.105011.

51 Q. Fu, Y. Meng, Y. Yao, H. Shen, B. Xie, Z. Ni and S. Xia, Construction of facet orientation-supported Z-scheme heterojunction of BiVO4 (110)-Fe2O3 and its photocatalytic degradation of tetracycline, *J. Environ. Chem. Eng.*, 2023, **11**, 111060, DOI: 10.1016/j.jece.2023.111060.

52 J. Zhu, J. Wang, J. He and L. Hu, Fabrication of CdS/ZnCr-LDH heterojunctions with enhanced of tetracycline hydrochloride photocatalytic degradation under visible light, *Opt. Mater.*, 2023, **136**, 113456, DOI: 10.1016/j.optmat.2023.113456.

53 Q. Gao, M. Wang, Y. Zhu, Y. Chai and B. Liu, A band structure modulated 1D/2D CdS/MgAl-LDH S-scheme heterojunction toward simultaneous photocatalytic removal of tetracycline and hexavalent chromium, *Appl. Surf. Sci.*, 2025, **693**, 162789, DOI: 10.1016/j.apsusc.2025.162789.

54 J. Zheng, Z. Zhao, J. Liang, B. Liang, H. Huang, G. Huang, M. Junaid, J. Wang and K. Huang, Simultaneous photocatalytic removal of tetracycline and hexavalent chromium by BiVO4/0.6CdS photocatalyst: Insights into the performance, evaluation, calculation and mechanism, *J. Colloid Interface Sci.*, 2024, **667**, 650–662, DOI: 10.1016/j.jcis.2024.04.127.

55 F. Li, Z. Fang, Z. Xu and Q. Xiang, The confusion about S-scheme electron transfer: critical understanding and a new perspective, *Energy Environ. Sci.*, 2023, **17**, 497–509, DOI: 10.1039/d3ee03282e.

56 S. Chen, L. Zhang, D. A. Alshammari, M. M. Hessien, W. Yu, L. Cui, J. Ren, Z. M. El-Bahy and Z. Guo, Z-scheme Ag2O/ZnO heterostructure on carbon fibers for efficient photocatalysis of tetracycline, *Sep. Purif. Technol.*, 2025, **354**, 129414, DOI: 10.1016/j.seppur.2024.129414.

57 S. Thakur, V. Mutreja, A. Tomar, S. Nainwal, K. Kaur, R. Kaur, Q. Li and F. S. Ataya, Phytochemical-assisted fabrication of ZrO2/ZnO nanocomposites: A sustainable approach for efficient photodegradation of tetracycline hydrochloride, *J. Mol. Struct.*, 2025, **1330**, 141350, DOI: 10.1016/j.molstruc.2025.141350.

58 L. Hongtanee, K. Wannakan, S. Nonthing, A. Panchakeaw, S. Nijpanich and S. Nanan, Solvothermally grown ZnO/BiOCl photocatalyst for solar-light-responsive degradation of tetracycline antibiotic, *OpenNano*, 2025, **25**, 100253, DOI: 10.1016/j.onano.2025.100253.

59 S. Nonthing, A. Panchakeaw, R. Dulyasucharit, H. Nakajima and S. Nanan, Fe3O4/BiOCl photocatalyst with magnetic recovery property for solar-light-responsive removal of Rhodamine B dye, *OpenNano*, 2025, **26**, 100260, DOI: 10.1016/j.onano.2025.100260.

60 T. senasu, N. Lorwanishpaisarn, K. Hemavibool, S. Nijpanich, N. Chanlek and S. Nanan, Construction of g-C3N4/BiOCl/CdS heterostructure photocatalyst for complete removal of oxytetracycline antibiotic in wastewater, *Sep. Purif. Technol.*, 2023, **306**, 122735, DOI: 10.1016/j.seppur.2022.122735.

61 T. Senasu, S. Nijpanich, S. Juabrum, N. Chanlek and S. Nanan, CdS/BiOBr heterojunction photocatalyst with high performance for solar-light-driven degradation of ciprofloxacin and norfloxacin antibiotics, *Appl. Surf. Sci.*, 2021, **567**, 150850, DOI: 10.1016/j.apsusc.2021.150850.

62 T. Senasu, T. Chankhanittha, K. Hemavibool and S. Nanan, Visible-light-responsive photocatalyst based on ZnO/CdS nanocomposite for photodegradation of reactive red azo dye and ofloxacin antibiotic, *Mater. Sci. Semicond. Process.*, 2021, **123**, 105558, DOI: 10.1016/j.mssp.2020.105558.